Ocean Engineering 246 (2022) 110625

Contents lists available at ScienceDirect

Ocean Engineering

journal homepage: www.elsevier.com/locate/oceaneng

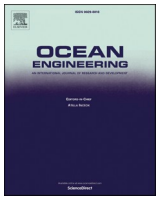

Using difference modelling and computational fluid dynamics to investigate the evolution of complex, tidally influenced shipwreck sites

Jan Majcher [a,*], Rory Quinn [a], Thomas Smyth [b], Ruth Plets [a,c], Chris McGonigle [a], Kieran Westley [a], Fabio Sacchetti [d], Mark Coughlan [e]

[a] School of Geography and Environmental Sciences, University of Ulster, BT52 1SA, Coleraine, Northern Ireland, United Kingdom
[b] School of Applied Sciences, University of Huddersfield, Queensgate, HD1 3DH, Huddersfield, United Kingdom
[c] Flanders Marine Institute, InnovOcean Site, Wandelaarkaai 7, 8400, Oostende, Belgium
[d] Marine Institute, Rinville, H91 R673, Oranmore, Ireland
[e] Irish Centre for Research in Applied Geosciences, O'Brien Centre for Science East, University College Dublin, Dublin, Ireland

ARTICLE INFO

Keywords:
Multibeam echosounder
Computational fluid dynamics
Shipwreck
Hydro-dynamics
Sediment-dynamics

ABSTRACT

The large number of historic metal-hulled shipwrecks on the seabed is a major consideration for the marine environment, heritage management and spatial planning. Their stability is driven by linked hydro- and sediment-dynamics, which in turn influence chemical corrosion and biological encrustation. The dynamism at underwater sites is frequently expressed in elaborate patterns of depositional and erosional features developed due to seabed scour. These settings are complex, due to the variable morphologies of the wrecks, and diverse types of seabed geology and geomorphology. Not only are the flow patterns and geomorphic changes at shipwreck sites not fully understood, but how these influence the wreck structures remains under-researched. Here we combine high-resolution multibeam echosounder, ocean current and sediment data with 3D Computational Fluid Dynamics (CFD) to investigate interrelations between hydro- and sediment-dynamics and the deterioration of two complex, fully submerged tidally-influenced shipwrecks. Intricate patterns of wake and horseshoe vortices are observed, and modelled wall shear stresses predict geomorphic changes recorded in 4-year and one-week interval difference models. Moreover, substantial damage is detected on the wrecks, correlated with areas of elevated wall shear stress and pressure in CFD simulations. The combined approach aids site management and provides analogies for offshore engineering.

1. Introduction

The wrecks of historic, metal-hulled ships are an integral part of the underwater landscape and new discoveries are made every year with increasingly sophisticated sensors and methodologies (Grządziel, 2020a, b; Geraga et al., 2020; McCartney, 2017, 2018; O'Toole et al., 2020; Plets et al., 2011). Many wrecks are archaeologically and historically significant, acting as time-capsules capturing contemporary technological advancements, life on-board and other information relevant for heritage science (Elkin et al., 2020; Firth, 2018). The UNESCO Convention on the Protection of the Underwater Cultural Heritage, adopted in 2001 (UNESCO, 2002) puts strong emphasis on *in-situ* preservation of underwater cultural heritage (defined as more than 100 years old). This is partly due to the vast extent of the submerged archaeological resource - currently estimated to number around 3,000, 000 wrecks worldwide (Croome, 1999; UNESCO, 2017) - which hinders costly active investigation and conservation measures.

The occurrence of shipwrecks on the seabed also has important ocean engineering implications. Upstanding wreck structures present complex obstacles to the water flow, locally modifying its magnitude and turbulence (Quinn, 2006). The seabed adjusts to these modifications and undergoes geomorphic changes, frequently forming intricate erosional and depositional signatures, referred to as scour or wreck marks (Caston, 1979; Majcher et al., 2020). The alignment of wreck marks along the dominant local current flow makes them proxies for magnitudes and directions of local hydrodynamic settings and net sediment transport (Caston, 1979). Wrecks of metal-hulled vessels lost up to the end of World War I have resided on the seabed for more than 100 years. Therefore examining the combined fluid-sediment dynamic response at such sites provides insights into potential issues with the stability of

* Corresponding author.
E-mail address: majcher-j@ulster.ac.uk (J. Majcher).

https://doi.org/10.1016/j.oceaneng.2022.110625
Received 10 September 2021; Received in revised form 10 December 2021; Accepted 14 January 2022
Available online 22 January 2022

other large and complex man-made structures after their long-term emplacement on the seabed.

Shipwrecks are often treated as impediments to offshore developments, leading to re-routing of undersea pipelines and cables and reconsideration of the placement of offshore infrastructure (Evans and Firth, 2016; Majcher et al., 2020). Therefore, using wrecks as indicators of the locally operating hydrodynamic and physical processes may be beneficial for ocean engineering, influencing marine spatial planners and stakeholders to recognise shipwreck sites as valuable elements of our maritime landscape. This is especially important in times of the rapid expansion of the offshore renewable energy sector and development of the seabed.

Geomorphic change at shipwreck sites is complex and depends on a range of local environmental factors and processes (Astley, 2016; Majcher et al., 2021; Quinn and Smyth, 2018). Precise hydrographic surveys using multibeam echosounders (MBES) combined with geophysical and geological sampling provides data essential to understand these variables (Bates et al., 2011; Plets et al., 2011; Westley et al., 2019). Such datasets are becoming increasingly available due to national and international seabed mapping programmes (EMODnet Bathymetry Consortium, 2018; Guinan et al., 2020; O'Toole et al., 2020). Furthermore, validated shelf-scale oceanographic models provide another layer of information, allowing insights into hydrodynamic triggers for geomorphic change (King et al., 2019; Nagy et al., 2020; Shchepetkin and McWilliams, 2005).

However, in order to understand the rates and magnitude of geomorphic change at shipwreck sites, at least two high-resolution hydrographic surveys, separated in time, are needed; an approach commonly referred to as repeat or time-lapse bathymetric surveying (Astley, 2016; Bates et al., 2011; Couldrey et al., 2020; Fernández-Montblanc et al., 2016; Majcher et al., 2021; Quinn and Boland, 2010). This strategy allows a comparison of the differences in bathymetric surfaces corresponding to consecutive surveys i.e., to conduct difference modelling. To date, investigations using difference modelling have confirmed a wide spectrum of geomorphic change affecting individual underwater sites (Astley, 2016; Fernández-Montblanc et al., 2016; Quinn and Boland, 2010), even for wrecks located at similar depths within a single, tidally dominated shelf-sea (Majcher et al., 2021). This variability in seabed dynamism indicates further research on possible factors controlling geomorphic change at wreck sites is required.

Numerical modelling is increasingly used in conjunction with hydrographic data to investigate detailed patterns of water flow and turbulence around manmade structures and to analyse factors driving geomorphic change and site evolution. For example, Couldrey et al. (2020) investigated how a barchan dune migrated past an offshore wind turbine monopile foundation using multi-annual repeat MBES surveys and a coupled sediment- and hydro-dynamic model. In another example, hydrodynamic modelling validated by *in-situ* observations and combined with repeat singlebeam bathymetric data was used to characterize sediment erosion and seasonal geomorphic changes at a scattered, partly buried and shallow, wave-dominated shipwreck site (Fernández-Montblanc et al., 2016). The investigation was later extended to 2D Computational Fluid Dynamic (CFD) simulations, using two different bathymetric profiles corresponding to high- (winter) and low- (summer) wave energy periods, providing insight into the effects of seasonality on local geomorphic change (Fernández-Montblanc et al., 2018). Extending these approaches to combining CFD with high-resolution MBES bathymetric data has the potential to further improve our understanding of the physical factors influencing stability of complex underwater structures like wrecks. This in turn can extend our knowledge of physical site formation processes (Ward et al., 1999). Even though successful CFD simulations have been carried out for wave-dominated (Fernández-Montblanc et al., 2018) and current-dominated (De Hauteclocque et al., 2007; Quinn and Smyth, 2018; Smyth and Quinn, 2014) wreck sites, none have been compared against high-resolution difference modelling from time-lapse MBES surveys.

Moreover, no comparisons of fluid dynamics and geomorphic change between individual wreck sites have been performed, either for sites located within similar or contrasting environmental settings. Finally, all CFD investigations published to date for shipwreck sites (Fernández-Montblanc et al., 2018; Quinn and Smyth, 2018; Smyth and Quinn, 2014) focus on older, pre-industrial wooden wrecks, and scattered (Fernández-Montblanc et al., 2018) or low-relief sites (Smyth and Quinn, 2014). Therefore hydrodynamic simulations around complex, upstanding, metal-hulled wrecks presenting significant obstacles to flow are unrealised.

This knowledge gap is highly relevant and important to address considering that there are 3 million shipwrecks estimated worldwide (Croome, 1999; UNESCO, 2017), with a significant portion originating from World War I and II. At least 8500 of these may contain oil and are classified as potentially polluting shipwrecks (Carter et al., 2021; Landquist et al., 2013). Understanding long-term stability, seabed geomorphic change and its drivers at metal-hulled shipwreck sites may enhance decision making processes in cultural heritage and pollution risk management, supporting marine spatial planning (Papageorgiou, 2018).

In this study we set out to extend the knowledge about the relations between hydro- and sediment-dynamics and the stability of complex, tidally influenced underwater structures. To do so, we analyse differences in geomorphic change and patterns of flow at two historic, metal-hulled shipwreck sites located within similar environmental contexts. The wrecks of HMS *Vanguard* and SS *W.M. Barkley* are both more than 100 years old (lost in 1875 and 1918 respectively), located in sand wave fields at depths of 40 and 52 m in the Irish Sea and with their hulls aligned oblique to tidal flows. Difference-modelling of very high-resolution time-lapse bathymetric data allows us to quantify multi-annual and weekly geomorphic change at the sites and compare the registered seabed changes to the CFD simulations. CFD is used to understand patterns of flow and turbulence at the sites. A shelf-scale oceanographic model provides tidal current velocity profiles for the inlets of the CFD domains. Finally, very dense MBES-derived point clouds enable evaluation of structural damage sustained by the wrecks. This unique combination of very high-resolution repeat bathymetric and modelled oceanographic data, together with seabed sampling and CFD simulations provides new insights into formation processes of underwater wreck structures. We believe that this study points to obvious analogies to offshore engineering and presents a new set of applications for high-resolution hydrographic and oceanographic data.

2. Theoretical background

Geomorphic change at shipwreck sites is largely driven by seabed scour. Scour occurs when sediment is eroded due to forcing by waves and/or currents (Whitehouse, 1998). It can be initiated by a change in morphology and/or migration of bedforms (Ginsberg and Aliotta, 2019; Hay and Speller, 2005; Soulsby, 1997) or by the intentional (e.g. seabed engineering; Whitehouse et al., 2011, unexploded ordnance, mines; Jenkins et al., 2007) or accidental (e.g. a shipwreck; Quinn, 2006) introduction of an object to the seabed.

When an object is introduced to the seabed it causes changes in the ambient flow regime, resulting in some combination of the following phenomena: streamline compression and acceleration of flow; formation of vorticial structures: a horseshoe vortex enveloping the structure and lee wake vortices downstream of the structure, occasionally accompanied by vortex shedding; increased flow turbulence and velocity; sediment liquefaction enhancing material loss (Quinn, 2006; Sumer et al., 2001). The seabed responds to this flow alteration and undergoes scour until a new equilibrium state with a maximum scour depth is reached (Soulsby, 1997; Whitehouse, 1998).

The horseshoe vortex is formed by the rotation of the seabed boundary layer. An adverse pressure gradient is formed by the structure, separating the flow, which consequently rolls up to form a swirling

vortex wrapped around it (Sumer et al., 1997; Whitehouse, 1998). The morphology of the horseshoe vortex can be variable, forming intricate flow patterns (like vortex shedding; Testik et al., 2005), especially at complex wreck structures (Quinn and Smyth, 2018). The lee wake vortices are created by the rotation of the boundary layer flow over the surface of the obstacle and brought together at some distance from it due to flow convergence (Testik et al., 2005). Two counter-rotating vortices may also form near the downstream side of the obstacle, depending on its morphology and orientation (Quinn and Smyth, 2018; Testik et al., 2005).

Two scour regimes are frequently distinguished in engineering (Whitehouse, 1998) and also recognized in shipwreck site characterization (Astley, 2016): live-bed and clear-water scour. These are defined in terms of the critical shear stress (τ_{cr}) required for incipient motion of sediments, and the bed shear stress (τ_c) exerted by the flow, both measured in Nm^{-2} or Pa in SI units. Live-bed conditions occur when τ_c exceeds τ_{cr} everywhere across the site, both inside and outside the scour signatures. On the other hand, the clear-water criterion is satisfied when τ_{cr} is exceeded only in the vicinity of the structure, where τ_c is amplified due to flow modification and not at the surrounding seabed. Both scenarios result in an equilibrium scour depth. However, while the clear-water scenario implies stability after the initial development of scour, the live-bed condition suggests continuous seabed dynamism. This is important in terms of the stability and preservation of underwater structures, especially for fragile objects like shipwrecks, which reside on the seabed over long time periods without any maintenance (Majcher et al., 2021).

Adverse effects due to the scour-induced geomorphic changes are well-known for underwater structures like bridges (Sumer, 2007), wind and tidal turbines (Matutano et al., 2013; Melling, 2015; Sun et al., 2019; Whitehouse et al., 2011) and jackup rigs (Sweeney et al., 1988). Sediment budget changes due to scour may also compromise the stability of shipwrecks, ultimately leading to partial or complete collapse and/or cause either burial or exposure of their corrosion-prone structures to the oxygenated water-column, enabling the development of biological encrustation (Quinn, 2006; Ward et al., 1999). Therefore, the importance of the scour phenomenon have been also recognized and extensively researched at shipwreck sites in the context of their *in-situ* preservation (Astley, 2016; Bates et al., 2011; Fernández-Montblanc et al., 2016, 2018; Majcher et al., 2020, 2021; McNinch et al., 2006; Plets et al., 2011; Quinn, 2006; Quinn and Smyth, 2018).

As upstanding, high-relief metal shipwreck structures frequently present substantial obstacles to flow, the scour signatures around them can be extensive (up to a few kilometres long; Garlan et al., 2015) and deep (up to several meters; Caston, 1979). The mechanisms guiding the temporal and spatial scales at which scour functions at shipwreck sites, are not yet fully understood and vary significantly between sites depending on local geological, geomorphological, geotechnical and oceanographic conditions and morphometric characteristics of the wreck itself (Astley, 2016; Majcher et al., 2021; Quinn and Smyth, 2018).

3. Materials and methods

3.1. Study sites

Two wrecks were investigated in the study: SS *W.M. Barkley* and HMS *Vanguard*. Both are located in the Irish Sea, a shelf basin characterized by dominating semidiurnal lunar (M2) and solar (S2) tides (Neill et al., 2014; Ozer et al., 2015). Surficial sediments in the Irish Sea mostly comprise reworked glacial and post-glacial substrates creating a complex mosaic of sediment types (Coughlan et al., 2020; Jackson et al., 1995; Ward et al., 2015). Continuous sheets of sand up to 40 m thick are present, frequently associated with migrating bedforms (i.e., sand waves) of various shapes, heights and spacings (Van Landeghem et al., 2009, 2012). Where sand supply is limited, a gravel lag deposit is exposed (Jackson et al., 1995). SS *W.M. Barkley* and HMS *Vanguard* are located in sand wave fields approximately 35 and 31 km east and south-east of Dublin respectively, approximately 19 km apart (Fig. 1). Depth-averaged, spring tide current velocities reach 1 m/s (Howarth, 2001) and previous studies have determined that the seabed is highly mobile in the area (Coughlan et al., 2021; Majcher et al., 2021), based on the data from the validated regional ocean modelling system (ROMS; Nagy et al., 2020). Sediments can be mobilised by tidal currents for 56% of the year around SS *W.M. Barkley* and 57% around HMS *Vanguard*, with waves having a limited influence on the sites due to their depth (52 and 40 m, respectively) (Coughlan et al., 2021; Majcher et al., 2021).

SS *W.M. Barkley* was the first steamship employed by Arthur Guinness and Sons Ltd., producers of Guinness stout. She sank on October 12, 1917 after a torpedo strike by the German U-boat *UC-75* while sailing from Dublin to Liverpool and resulted in the loss of four lives (Brady et al., 2012). HMS *Vanguard* was an *Audacious*-class ironclad battleship. On September 1, 1875 HMS *Vanguard* was sailing from Dublin to Queenstown (Cobh) with six other battleships, when the formation encountered fog and *Vanguard* was accidently rammed by her sistership HMS *Iron Duke*, resulting in sinking with no loss of life (Brady et al., 2012). Both wrecks are more than 100 years old and protected in Ireland by the National Monuments Act (National Monuments Service, 1987).

3.2. Oceanographic data

Depth-averaged current velocity magnitudes and directions were obtained for the area covering the wreck sites from an operational model run by the Marine Institute of Ireland (Nagy et al., 2020). The model is an implementation of the Regional Oceanic Modelling System (ROMS; Shchepetkin and McWilliams, 2005) for an area of the NE Atlantic encompassing Irish waters. The temporal resolution of the model data is hourly and the horizontal resolution in the Irish Sea ranges from 1.1 to 1.7 km. Model data used in this study cover a 1-year period (January 31, 2019–December 31, 2019) and were used for site characterization to provide current roses and to establish inlet current velocity profiles for the CFD simulations.

3.3. Repeat hydrographic surveys

High-resolution repeat hydrographic surveys were conducted in September 2015 and October/November 2019 to provide data for site characterization and detection of geomorphic and structural changes over a 4-year interval. Additionally, in 2019, two hydrographic surveys spaced 1 week apart were conducted at the SS *W.M. Barkley* site. The first survey (26 October) took place before a spring tide (28 October) and a storm (29 October – 3 November) after which the second, repeat survey was conducted (3 November). Westley et al. (2019) and Majcher et al. (2021) provide comprehensive descriptions of the survey methods and strategies used to collect the high-density, detailed, shipwreck-focused and repeat regional MBES data used for assessing structural and geomorphic changes respectively. Only the key parts of these methods are described here, for brevity, and more details are included in the supplementary material.

Bathymetric and backscatter data were collected onboard RV *Celtic Voyager* using a hull-mounted MBES. The bathymetric data were processed in CARIS Hips and Sips v. 9.1 software, including point cloud cleaning and tidal and refraction corrections. Quality control using crosslines showed >98% compliance with the IHO Special Order standard (IHO, 2020). The processed datasets were exported to rasterized digital elevation models (DEMs) in the UTM 30N projection with a common 0.3 m pixel size (i.e., spatial resolution) and clipped to the extents of CFD domains. The backscatter data were imported to QPS Fledermaus Geocoder Toolbox (FMGT v.7.8.9) and corrected for angular varying gains with 25% of the nadir zone blended between lines to reduce artefacts (Lurton and Lamarche, 2015). Backscatter intensity mosaics were then generated at 0.3 m spatial resolution.

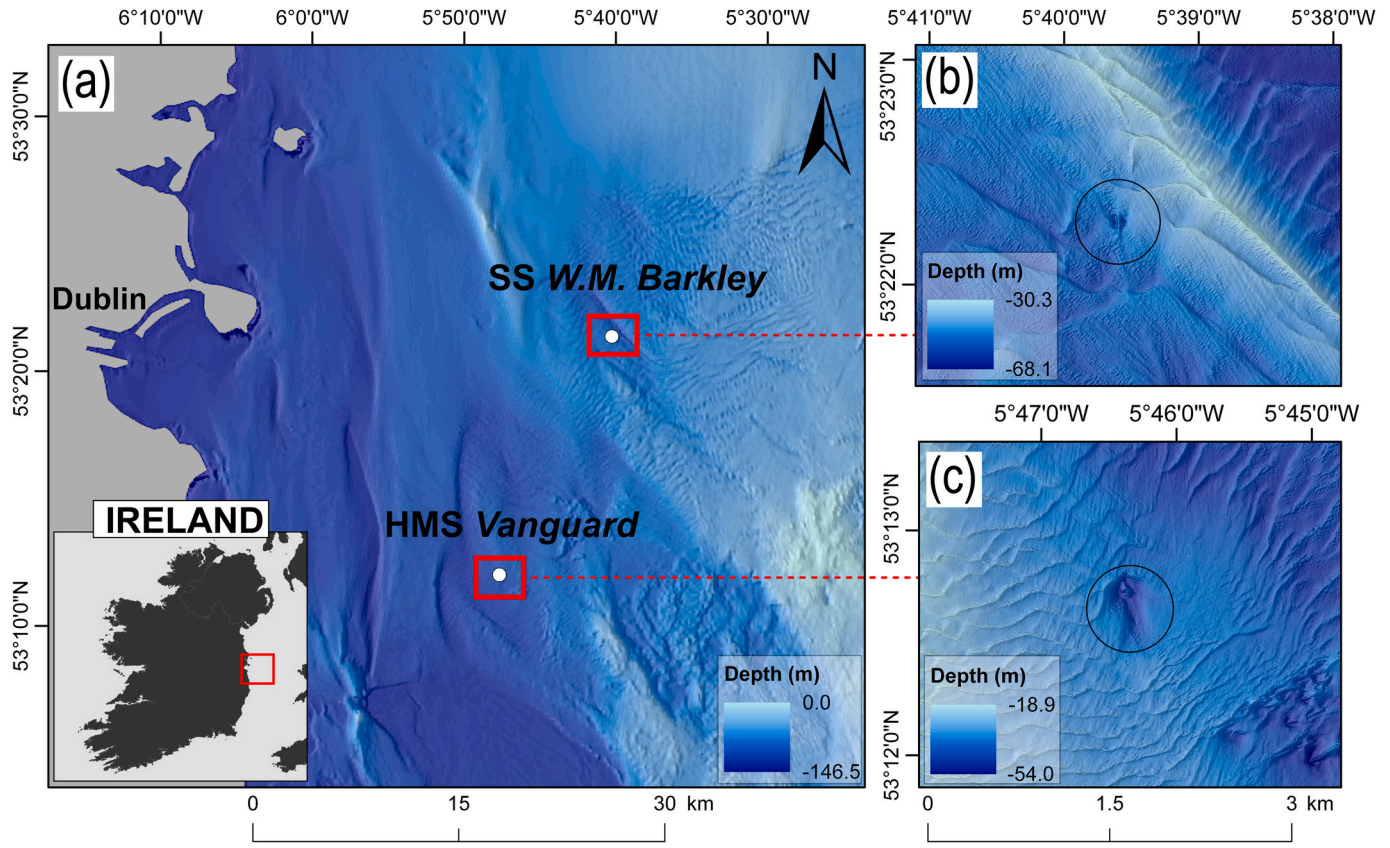

Fig. 1. (a) Location of the study area and the (b) SS W.M. Barkley and (c) HMS Vanguard sites. Backdrop bathymetry was obtained from (a): EMODnet (EMODnet Bathymetry Consortium, 2018); (b) and (c): INFOMAR project (Guinan et al., 2020).

The regional acquisition strategy for site characterization and geomorphic change detection was designed specifically to capture the shipwreck sites and the surrounding seabed including the full extent of observed scour signatures at high resolution, using the same, consistent equipment setup between the consecutive surveys (Majcher et al., 2021). On the other hand, the high-density, detailed acquisition strategy was used to assess structural changes at shipwrecks and involved multiple slow passes over the wrecks to capture dense point clouds (MCA, 2018; Westley et al., 2019). Rapidly changing weather conditions and time constraints did not allow us to apply the detailed strategy to the SS *W.M. Barkley* during the 2019 survey. Hence, the assessment of structural changes for this site compares the 2015 detailed survey data with the 2019 regional survey data plus a cross line running over the wreck.

3.3.1. Site characterization

The regional bathymetric and backscatter datasets collected in 2015 were used for site characterization. The DEMs of HMS *Vanguard* and SS *W.M. Barkley* were imported into ESRI ArcMap 10.7.1 GIS software, where erosional and depositional signatures were delineated following Majcher et al. (2020). The shipwrecks' dimensions, morphometry of sand waves and scour dimensions and depths were obtained using GIS measuring tools. Migration directions of sand waves were determined from their asymmetric profiles (Van Landeghem et al., 2009, 2012). Slope layers were derived from the DEMs to enhance morphometric description of the scour signatures.

3.3.2. Structural change

CloudCompare v. 2.11.3 software was used to assess structural changes on the wrecks between 2015 and 2019, by comparing dense point clouds. The point clouds were initially imported and cropped to the same extents encompassing a box around the wrecks. Their volumetric densities were calculated using the Compute Geometric Features tool. Signed differences between the 2015 and 2019 point clouds were obtained using the M3C2 plugin (James et al., 2017), taking into account the ± 0.3 m vertical positioning uncertainty. The resulting difference scalar fields were projected onto the point clouds of SS *W.M. Barkley* and HMS *Vanguard* obtained in 2015.

Cleaning multibeam echosounder-derived point clouds collected over shipwrecks is not straightforward, as parts of their complex structures may be confused with noise. Therefore, the data from the M3C2 analysis were carefully examined for false indicators. Discrepancies were checked by superimposing the two consecutive point clouds for each wreck and visually assessing whether a difference could be attributed to a real event or to acquisition artefacts. The ambient occlusion ShadeVis plugin and the EyeDome Lighting OpenGL shader were applied together to enhance the comparisons and visualization of the point cloud data.

3.3.3. Geomorphic change

To perform difference modelling, the 2015 and 2019 regional DEMs of HMS *Vanguard* and SS *W.M. Barkley* were imported into ArcMap 10.7.1 software and used with the Geomorphic Change Detection (GCD) Addin for ArcGIS (Wheaton et al., 2010). The resulting 0.3 m resolution difference models represent geomorphic change between 2015 and 2019 for both wrecks, and additionally over a one-week interval in 2019 for SS *W.M. Barkley*. Percentages of erosional and depositional change were calculated based on pixel values in the difference models. Pixels within the ± 0.3 m vertical range were excluded from the analysis, as they were within the vertical uncertainty calculated by the CUBE algorithm (Calder and Wells, 2007; Majcher et al., 2021), except for the visualization of the short-term difference model for the SS *W.M. Barkley* site, where majority of the change was of low magnitude.

3.4. Sediment samples

Sediment samples were collected using a Shipek grab inside and outside the erosional and depositional signatures. Granulometric analysis of the sediments was performed using a MALVERN Mastersizer 3000 laser diffraction particle size analyzer for samples collected at the SS *W. M. Barkley* site and using a sieve stack for the HMS *Vanguard* samples. Sediment classification into Folk classes (Folk, 1954) and median grain size (d_{50}) calculations were performed using Gradistat v. 8 software (Blott and Pye, 2001).

3.5. Flows at the sites - computational fluid dynamic simulations

3.5.1. Stereolithography geometry

CFD simulations were conducted using triangular meshes constructed using DEMs and dense point clouds from the 2015 MBES surveys. The Poisson Surface Reconstruction plugin (Kazhdan et al., 2006) in CloudCompare was used to triangulate the MBES data and export the obtained meshes as stereolithography (.stl) files. The files were then imported to the Autodesk Meshmixer v. 3.5.474 software for quality checks and smoothing of mesh artefacts. The meshes covered a stretch of the seabed approximately 900 m long and 200 m wide, with the shipwrecks in the middle (Fig. 2). The direction of the longer sides of the rectangular domains was the same as the direction of the inlet tidal

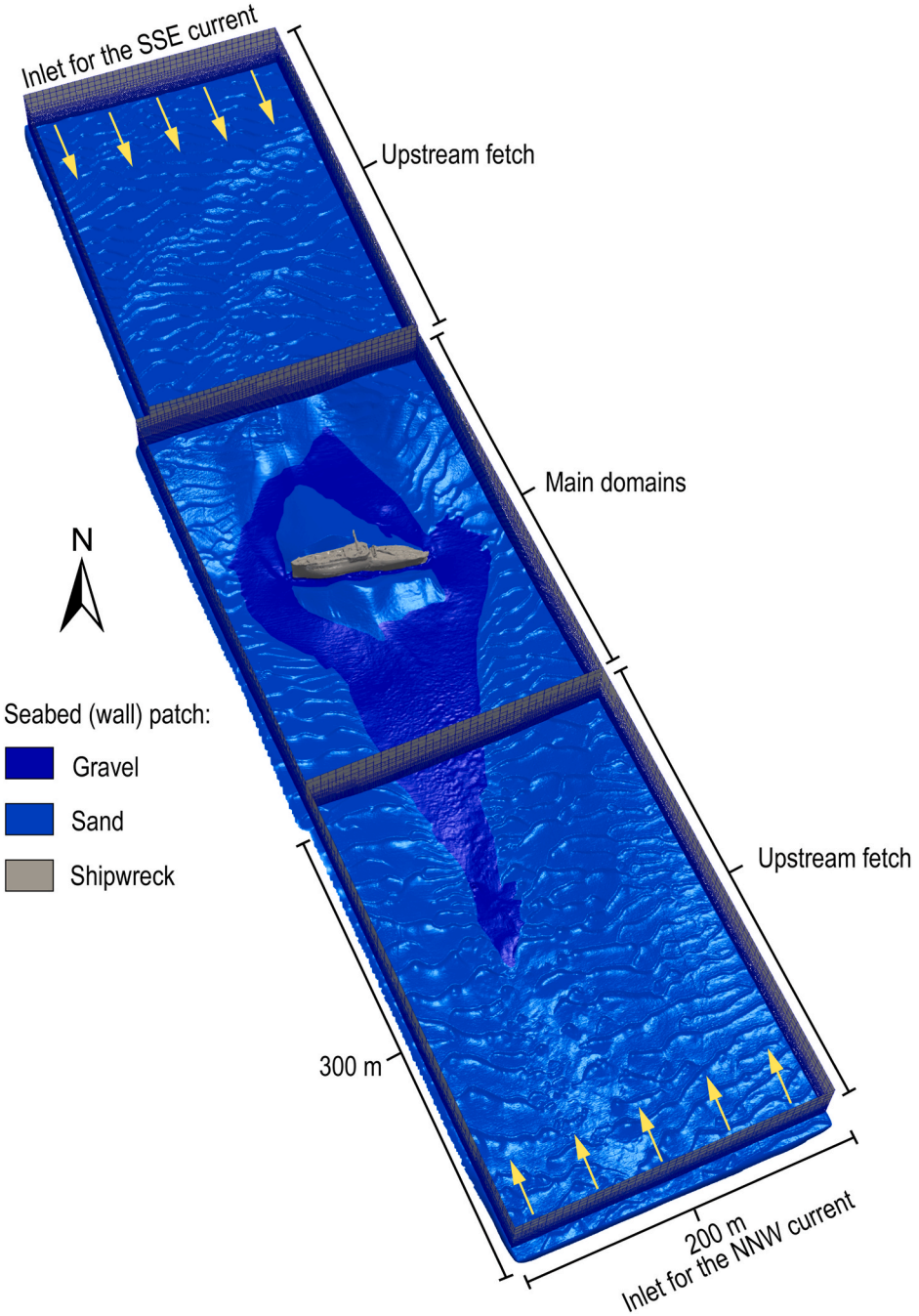

Fig. 2. CFD mesh setup for the HMSVanguard site including the upstream fetch domains for both simulated current directions and the main domains with the shipwreck site. SS W.M. Barkley site's mesh setup is analogous, except the sand-grain roughness height parameter was set as uniform.

current for each mesh.

For SS *W.M. Barkley*, a DEM with a spatial resolution of 0.3 m (from the regional survey) was used to represent the seabed around the wreck, which was merged with a finer DEM of 0.1 m resolution (from the detailed survey) encompassing the wreck. The resulting point cloud was then triangulated. The hull of HMS *Vanguard* is better preserved than that of SS *W.M. Barkley*, with most of its structure standing proud of the seabed. This complex structure, which includes well-preserved discrete structural elements (e.g. a collapsed mainmast), necessitates fully 3-dimensional rendering of the site (rather than 2.5-dimensional provided by DEM representation). Therefore, additional points were added to the DEM points from the non-gridded, dense point cloud obtained during the detailed survey to represent parts of the hull and the collapsed mast, which would otherwise be obscured using only the regularly gridded DEM data. Using these detailed point clouds to represent the entire wrecks was deemed unfeasible, due to their high irregularity causing triangulation problems.

3.5.2. Simulation setup and initial conditions

OpenFOAM v.6 (Weller et al., 1998) was used for creating computational domains (or CFD meshes) and simulating flows. ParaView v. 5.9.0 was used for processing and visualization of the CFD results. The OpenFOAM code solves Reynolds-averaged Navier–Stokes (RANS) equations using the finite volume method. Three-dimensional CFD RANS simulations of water flows over complex terrain using the OpenFOAM code have been previously validated against and have shown good agreement with experiment data (for example for riverine flows over dunes: Unsworth et al., 2020). Additional remarks on the validation of simulations with experiment data are included in the supplementary material. Main simulations were run in parallel on 80 processors on the high-performance computer facility at Ulster University. Second-order accuracy schemes were used to translate governing partial differential equations into algebraic equations, solved within the computational domains. OpenFOAM's Geometric-Algebraic Multi-Grid solver (GAMG) was used for the Poisson equation for pressure and the Stabilised Preconditioned (Bi-) Conjugate Gradient (PBiCGStab) (Van Der Vorst, 1992) for all other equations.

Details about the RANS equations can be found in Versteeg and Malalasekera (2007). Flow fields were calculated using the shear-stress transport (SST) k-ω turbulence closure (Menter et al., 2003), previously used for flow simulations at shipwreck sites (De Hauteclocque et al., 2007; Fernández-Montblanc et al., 2018) and for analogue problems like solving turbulent flows around tidal turbines (Shives and Crawford, 2014; Sun et al., 2019) and sand dunes (Liu et al., 2021). The inlet turbulence kinetic energy k, and specific dissipation rate ω, were estimated according to the equations included in the supplementary material (OpenCFD Ltd., 2019; Simpson et al., 1996).

Directions and magnitudes of the inlet tidal currents were obtained using the ROMS model outputs (see section 3.2). Specifically, the 90th percentiles of the current magnitudes for two main directional lobes of the current roses (tidal currents are strongly bi-directional at the sites) were extracted from the data and used at the inlets, as they were determined to represent spring tide current speeds accurately. Mean directions of the currents exceeding the 90th percentiles of current magnitudes (speeds) within these two directional lobes were calculated and used as the inlet current directions. Current velocity profiles were then calculated using the depth-averaged velocity magnitudes according to the empirical formula provided by Soulsby (1997) (see supplementary material).

As the flow becomes unsteady around underwater obstacles (e.g., Roulund et al., 2005), simulations of such flows at shipwreck sites usually use transient solvers (De Hauteclocque et al., 2007; Quinn and Smyth, 2018; Smyth and Quinn, 2014). In this paper, the Pressure Implicit with Splitting of Operators (PISO) algorithm (Issa, 1986), which maintains unsteady components of the flow, was used. Time-steps were assigned in such a way that the maximum Courant number never exceeded 0.3. Simulations were considered converged when the calculated initial residuals, measuring the local imbalances of conserved variables in control volumes, dropped below 1e-05 or levelled-off.

The 3D computational domains were created using the OpenFOAM's native mesh generator, SnappyHexMesh, which is capable of incorporating stereolithography files into CFD meshes. The meshing strategy generally followed the previously established workflows for 3D CFD simulations at shipwreck sites (Quinn and Smyth, 2018; Smyth and Quinn, 2014), with a gradual increase in refinement with a decreasing distance to the seabed (i.e., cells are the finest close to the seabed) and with the same boundary conditions applied. Additional refinement boxes were added to provide greater refinement of the mesh cells corresponding to shipwreck structures and the water mass up to approximately 5 m above them. Three layers were extruded adjacent to the shipwreck/seabed geometries to provide further refinement of the near-wall region.

In order to model realistic inlet conditions and develop flows for the main simulations (Blocken et al., 2015; Wakes, 2013), the flows were initially simulated at a coarse resolution (approximately 2.7 million cells) at extended domains over the seabed, captured using the regional hydrographic survey strategy (referred to as upstream fetch domains). The stereolithography files were subdivided into three parts in such a way that the first part corresponded to the upstream fetch of one tidal current direction, the second part to the main domain containing the shipwrecks and the third part to the upstream fetch of the opposite tidal current direction (Fig. 2). Hence, four simulations were conducted for each site: two for each current direction. The first simulation of each current direction regime was simulated at the upstream fetch domain corresponding to that direction, and all the flow fields were then mapped from its outlet to the inlet of the second, main domain. The main domains were designed in such a way that their widths and the lengths of the downstream zones exceeded 15 and 5 mean heights of the shipwrecks, accordingly, to exclude the influence of CFD domain size on the simulations (Blocken, 2015). Additionally, grid independence tests were carried out by performing simulations using grids with increasing numbers of cells: 2.1, 5.0 and 13.4 million cells and 4.5, 7.3 and 12.1 million cells for the SS *W.M. Barkley* and HMS *Vanguard* sites, respectively. Comparison of flow characteristics for the simulations demonstrated that differences related to grid resolution were irrelevant for the purpose of the investigation (see details in the supplementary material).

The results of the granulometric analysis of sediment samples (presented in sections 4.1.1. and 4.2.1.) guided the choice of the sand-grain roughness height parameter, k_s for the seabed wall patch. This parameter is defined as $k_s = 2.5d_{50}$, where d_{50} is the median grain parameter (Soulsby, 1997). As sediments are uniform at the SS *W.M. Barkley* site, a uniform k_s was imposed at the seabed wall patch. At the HMS *Vanguard* site, the seabed wall patch was segmented into regions of different k_s based on the sediment grab information and manual classification of the backscatter data (section 4.2.1).

3.5.3. Flow patterns

Flow streamlines were extracted near the seabed using velocity components, time-averaged over 100 s windows, to visualize flow patterns over the wreck sites. Additionally, in order to define vortices objectively, iso-surfaces of the Q values were rendered for the sites. The Q-criterion, expressed in s^{-2}, defines vortices as areas where the Euclidean norm of the vorticity tensor, Ω, dominates that of the rate of strain S (Hunt et al., 1988): $Q = (|\Omega|^2 - |S|^2) > 0$.

3.5.4. Sediment mobility and wall shear stress

Mobility of sediments can be evaluated by comparing two variables: wall (or bed) shear-stress (τ_c) exerted by the flow and the critical shear stress which is specific to the sediment type (τ_{cr}). In OpenFOAM, the flow-related wall shear stress (τ_c) can be calculated using a built-in function, and is retrieved from the Reynolds stress tensor, resolved in

the direction normal to each face of the wall patch (OpenCFD Ltd., 2019). In our modelling, the simulated τ_c values were time-averaged using a 100 s window after the convergence criteria were met, to represent determinative flow conditions. The calculation procedure (Whitehouse, 1998) for the critical shear stress, τ_{cr} is provided in the supplementary material.

Whenever $\tau_c > \tau_{cr}$, the sediment mobility criterion is met (Whitehouse, 1998). Therefore, in order to determine the areas prone to sediment mobility, the simulated and time-averaged wall shear stress values were exported as.csv files from ParaView for both sites, gridded as mosaics at the 0.3 m spatial resolution, compared against the critical shear stresses and represented on maps in GIS. The simulated τ_c distributions were also used to discuss the influence of flows on structural changes sustained by the wrecks.

4. Results

4.1. SS W.M. Barkley

4.1.1. Site characterization

SS *W.M. Barkley* is broken into two pieces and lists to starboard, with her bow detached from the torpedo strike (Brady et al., 2012). The main hull section measures 49 × 10 × 8 m, and the detached bow section 23 × 10 × 5 m. The shipwreck is surrounded by a scour pit, extending 285 m to the NNW and reaching a maximum depth of 13.96 m (in 2015, relative to the surrounding seabed) at approximately 4 m distance from the detached hull (Fig. 3a). This erosional signature is asymmetric, more developed in the NNW direction than SSE and divided by a depositional ridge, which intersects the wreck midships, causing partial burial. Similar signatures are not clearly defined in the backscatter data, suggesting sediments are nearly uniform across the site (Fig. 3b). Variations in the backscatter intensity are attributed to the variable slopes and acoustic shadows associated with pervasive sand waves. The seabed slopes steeply within the scour signatures, with gradients exceeding 30° (Fig. 3c).

Granulometric analysis of the grab samples confirms that the sediments are uniform across the site, comprising medium sand (average d_{50} = 0.302 mm). The bathymetry around the wreck is variable, with sand waves dominant. Bedforms, with typical wavelengths of 10–15 m and heights of 0.5–1.0 m, are aligned to the dominant depth-averaged current directions (NNW-SSE) derived from the regional ocean model, with maximum currents of 0.94 m/s. Sand waves' asymmetry indicates that

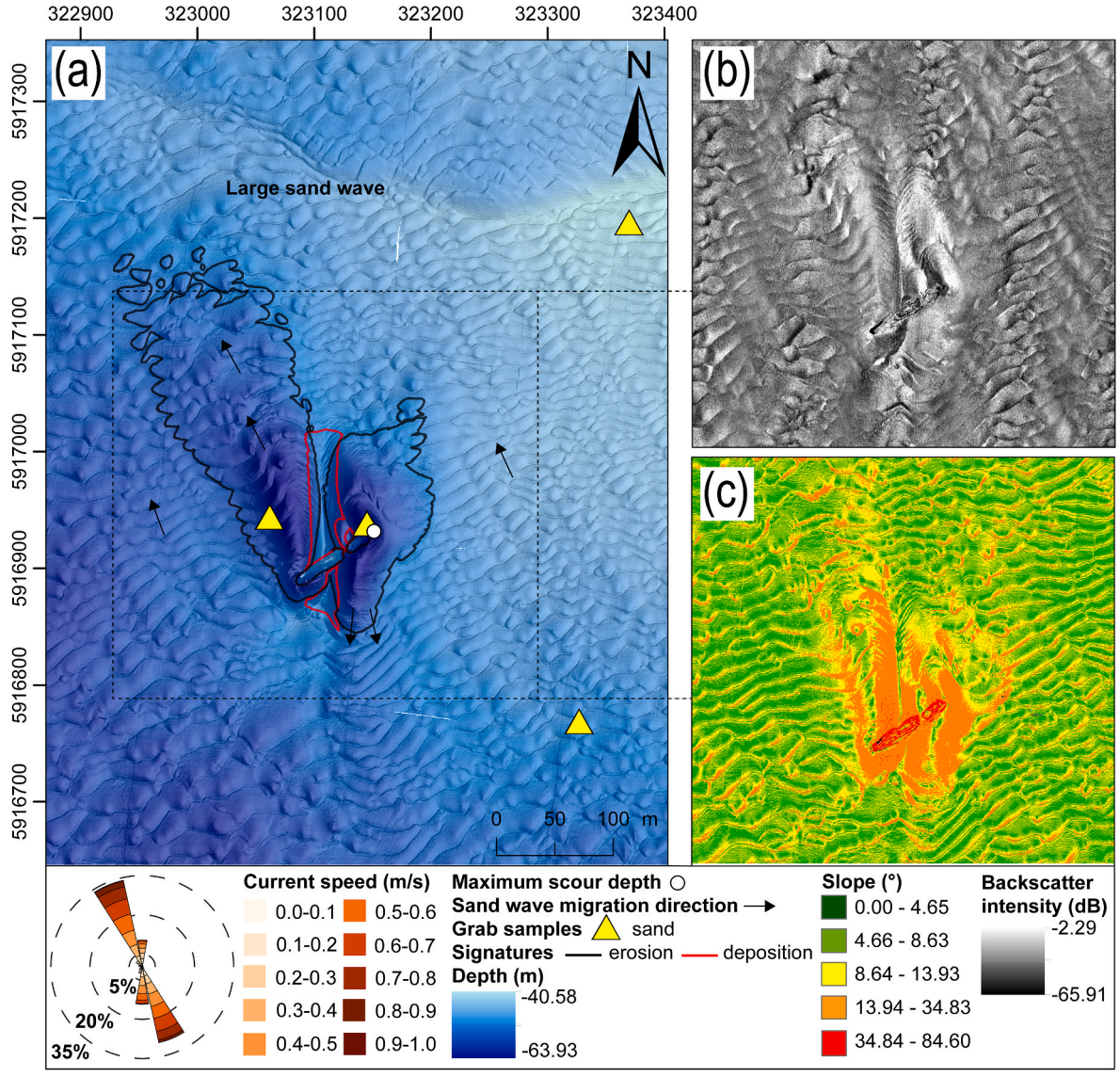

Fig. 3. Site characterization of the SS W.M. Barkley site. (a) Bathymetric DEM with the current rose obtained from the regional oceanographic model, (b) backscatter intensity mosaic, (c) slope map segregated using Jenks natural breaks optimization.

the majority propagate with the stronger NNW-directed tidal current. Notably, the propagation is reversed in the scour pit SSE of the wreck (Fig. 3a). A large, presumably relict sand wave (not aligned with the currents) is present to the north of the wreck, with an approximate height of 4 m.

4.1.2. Geomorphic change

The high-resolution bathymetric surveys conducted at the SS *W.M. Barkley* site allowed for evaluation of both long-term (2015–2019: Fig. 4a and b) and short-term (one week: Fig. 4c and d) differences in bathymetry.

High-magnitude differences reaching up to −4.9 m and +3.0 m are observed around the site in the long-term difference model (Fig. 4a) and are associated not only with sand wave migration, but also reorganisation of sediments within the erosional and depositional signatures. Notably, the location of the maximum scour depth moved farther north from the wreck, by approximately 4 m and was 1.01 m deeper. The largest changes occurred in the pits located in immediate proximity to the wreck. In terms of areal coverage, negative change (38.5% of the area) is more extensive than positive change (21.6% of the area), suggesting that the site is in a state of net erosion (Fig. 4b). The calculated mean bathymetric change (−0.17 m) also suggests net erosion.

Significant bathymetric changes are observed at the site even in the short-term (one week) difference model (Fig. 4c). Retaining pixels within the vertical measurement uncertainty (±0.3 m) highlights sand wave migration everywhere across the site. The migration is clearly enhanced to the NNW and SSE of the wreck, corresponding to downstream regions of the tidal currents, where changes of the highest magnitude for this interval were recorded, exceeding the measurement uncertainty (up to ± 0.5 m). The mean bathymetric change for this interval is also negative, however, as shown in Fig. 4d, most of the change (99.2%) fits between ± 0.3 m. Hence, any statistical quantification (including areal percentage calculations) for these short-term changes is deemed unreliable.

4.1.3. Structural change

Structural change was assessed through point cloud comparisons. The mean number of points within 1 m radius spheres (volumetric density) of the point clouds obtained for SS *W.M. Barkley* in 2015 and 2019 was 1037 and 46, respectively. Point cloud density from 2019 is significantly lower as weather conditions did not allow a high-density survey. Nevertheless, both point clouds successfully capture all the main structural elements of the wreck (Fig. 5a and b), including a counter stern, funnel hole, gunwales and other intricate details.

The M3C2 difference model highlights two regions of major structural change: the detached bow section and the portside gunwale of the counter stern (Fig. 5c). Examination of the difference model (Fig. 5c, box 1) indicates that a significant portion of the gunwale collapsed and is now hanging from the portside, leaning against the seabed (Fig. 5b). Differences noted at the bow (Fig. 5c, box 2) (and elsewhere) may be associated with disparities in point cloud densities and subjective cleaning of the point cloud during data processing. The bow structure is highly complex with multiple protruding elements, making point cloud cleaning difficult.

4.1.4. Sediment mobility and wall shear stress

Analysis of sediment samples indicate uniform sand (mean d_{50} = 0.302 mm) at the SS *W.M. Barkley* site, and an equivalent uniform k_s was

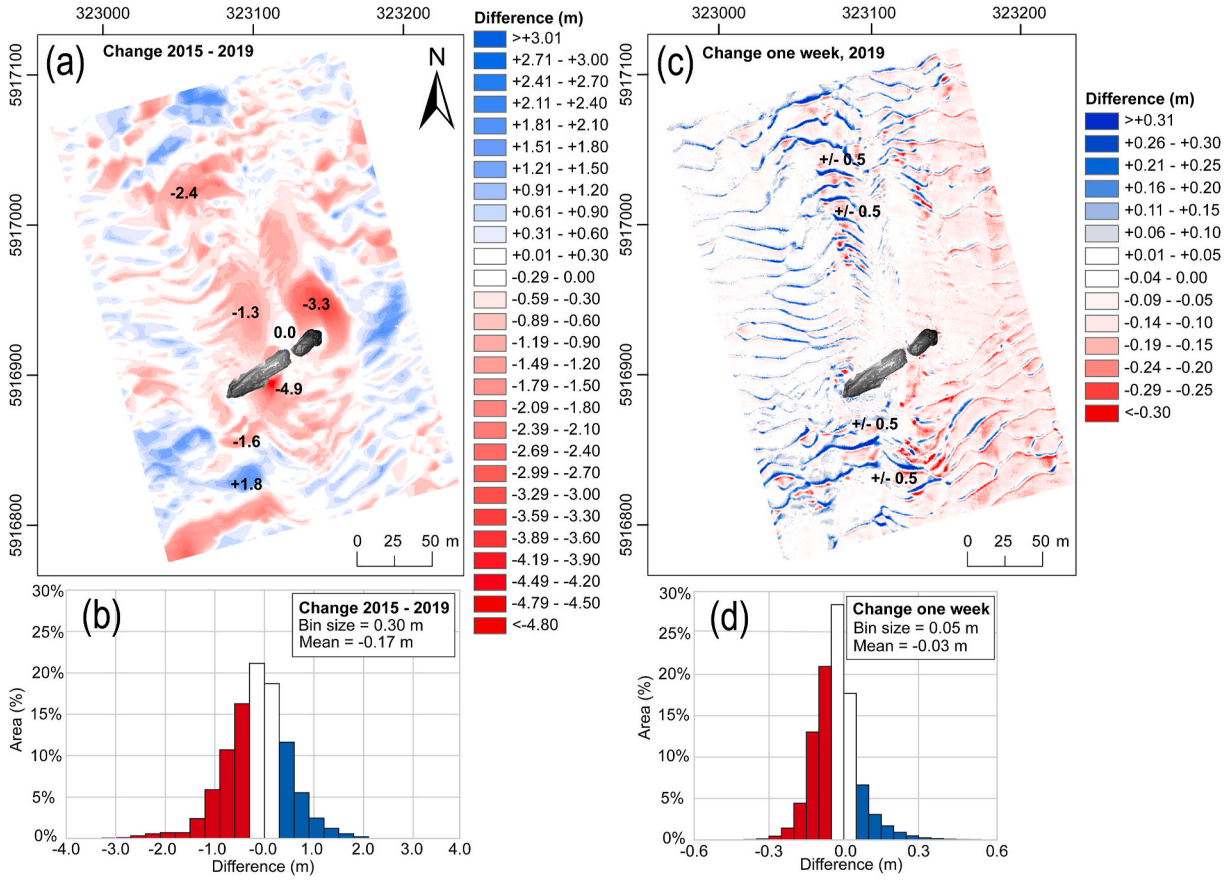

Fig. 4. Difference models for the SS W.M. Barkley site. (a) long-term model (2015-2019), (b) areal percentage histogram for the long-term model, (c) short-term model (one week, 2019), (d) areal percentage histogram for the short-term model. Numbers on the difference models represent localised changes. Note that the bin sizes for the histograms are different.

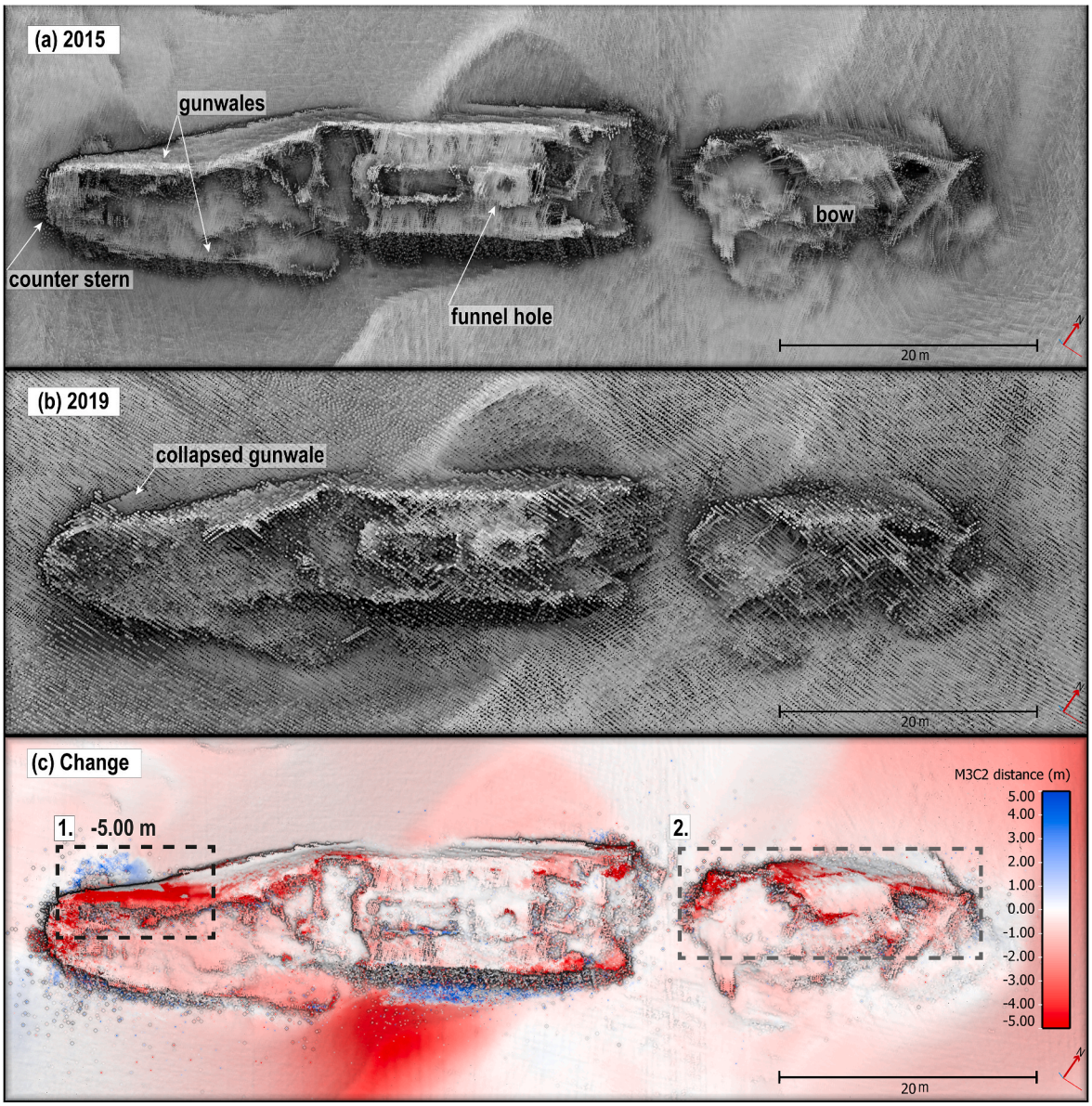

Fig. 5. Structural change model for the SS W.M. Barkley site. (a) point cloud corresponding to the 2015 survey , (b) point cloud corresponding to the 2019 survey, (c) difference model for the interval 2015-2019. Black and grey dashed lines represent certain and uncertain changes respectively.

imposed at the seabed wall patch for the simulations. The extracted 90th percentiles of depth-averaged current speeds are 0.77 m/s and 0.74 m/s for the NNW and SSE directions and were imposed at the inlets to the computational domains.

The resulting wall shear stress maps for both current directions are presented in Fig. 6. Three τ_c groups were empirically distinguished, based on the areal frequency distributions of the values and the critical shear stress value, τ_{cr} (0.19 Pa): low, which comprises values below the τ_{cr}; moderate, comprising values between the τ_{cr} and three times larger (0.19–0.58 Pa); and high containing all the values above 0.58 Pa.

The sediment mobility criterion is met ($\tau_c > \tau_{cr}$) across the site, indicating sediment is mobilised under the simulated current regimes (Fig. 6a and c) with 90.1% of the area experiencing the critical shear exceedance under the NNW regime (Figs. 6b) and 68.0% under the SSE current (Fig. 6d).

For the NNW current, τ_c is heavily modified at the lee side of the wreck, with an elongated high magnitude zone stretching from the stern toward the NNW and a low magnitude shadow zone extending from midships and from the detached bow (Fig. 6a). Additionally, τ_c is substantially elevated on the crests of the sand waves everywhere across the site, in particular SE of the wreck (Fig. 6a). τ_c is also amplified on the lee side of the wreck under the SSE current, with the highest level of magnitude adjacent to the midship section. Mean τ_c values calculated for both current directions (0.47 Pa for the NNW current and 0.27 Pa for the SSE current), together with distribution of values (Fig. 6 c and d), suggest that overall the NNW current regime is associated with significantly higher bed shear stresses than the SSE current regime.

With respect to the distribution of τ_c at the shipwreck itself, the parts of the wreck structure standing high above the seabed are exposed to the highest shear stresses under both current regimes (Figs. 6a, box 1 and 6c, box 1). Under the NNW current, the highest τ_c is modelled at the ship's portside gunwale near the counter stern (Fig. 6a, box 1). The detached bow also experiences elevated wall shear stress. Under the SSE current, τ_c is increased midships and at the detached bow (Fig. 6c, box 1).

4.1.5. *Flow patterns*

The simulated NNW and SSE currents are orientated at 69° and 68° to the SS *W.M. Barkley*'s broken hull. Fig. 7 shows fully developed,

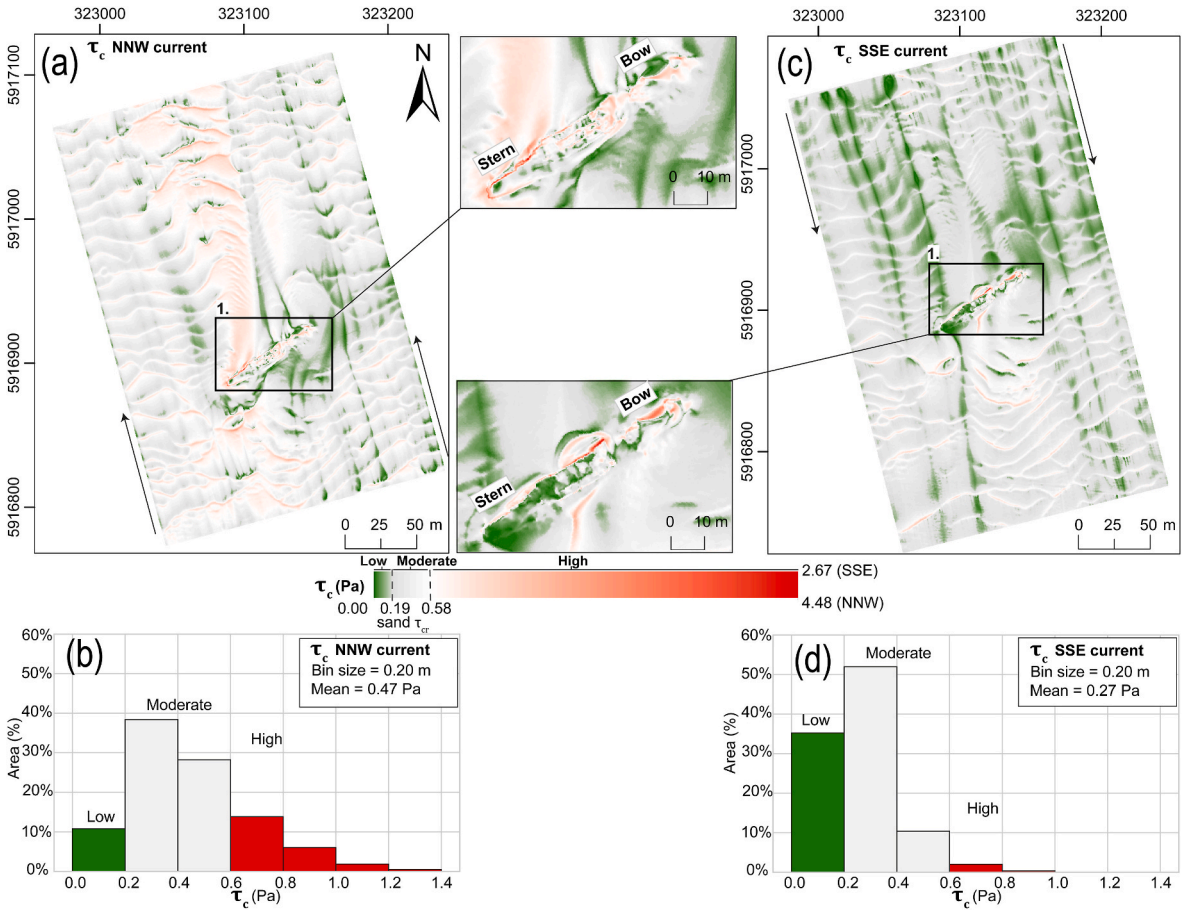

Fig. 6. Simulated wall shear stress maps for the SS W.M. Barkley site. (a) Wall shear stress under the NNW current with (1) close-up on the wreck, (b) areal percentage histogram for the wall shear stress values under the NNW current, (c) wall shear stress under the SSE current with (1) close-up on the wreck, (d) areal percentage histogram for the wall shear stress values under the SSE current.

averaged flow patterns at the site represented with flow streamlines and Q value iso-surfaces at Q = 0.0001 s^{-2}. Intricate flow patterns are developed around the complex structure of the wreckage. An irregular horseshoe vortex is developed around the main body of the wreck, but not around its bow under the NNW current (Fig. 7a and b). The right leg of the vortex passes through the gap between the broken midship part of the wreck and the detached bow, and the left leg terminates at the counter stern (Fig. 7b). Both legs appear to merge with complex vorticial patterns developed in the wake of the shipwreck (Fig. 7b). The wake vortices are generally characterized by a strong asymmetry; the stern-originating (inflow) vortices are more developed than the bow-originating ones. At least two wake vortices extend from the wreck's main structure; one closer to the stern and one closer to midships. They merge downstream in proximity to the wreck to form a single wake vortex stretching along the side of the depositional ridge (Figs. 7b and 3a). Another, less pronounced wake vortex is developed at the bow part, getting closer to the larger in-flow wake vortex with increasing downstream distance over the opposite slope of the depositional signature (Fig. 7a and b).

Under the SSE current, a horseshoe vortex is formed only at midships (Fig. 7d), on one side climbing the depositional ridge, which partially covers the wreck, and passing through the bow-midship gap on the other side. Similar to the patterns developed under the NNW current regime, the incoming SSE current causes the development of separate wake vortices over the bow and the main part of the wreck. Here, the inflow, bow-originating vortex seems to be less developed than the larger midship-stern originating vortex.

4.2. HMS Vanguard

4.2.1. Site characterization

HMS *Vanguard* lists to starboard, measures 90 × 20 × 12 m in the maximum length, width, and height, respectively. An extensive, comet-shaped scour pit is developed at the site, with its main body stretching up to 280 m SSE of the wreck (Fig. 8a). The erosional influence of the shipwreck on the seabed, however, can be observed at a larger distance, exceeding 400 m (Fig. 8a). The scour pit is asymmetric, developed more towards the SSE, with a maximum depth of −11.69 m at the stern section, and a depth of −11.60 m at the bow section (white dots on Fig. 8a). A streamlined depositional zone is delineated proximal to the wreck, extending in both directions along the main axis of the pit.

The main part of the scour pit stands out in the slope map as it is nearly flat compared to the highly variable surrounding bed (Fig. 8c). No sediment grabs were retrieved from the erosional zone despite three sampling attempts, suggesting coarse sediment is exposed here by erosional processes. This interpretation is supported by seismic profiles (Majcher et al., 2021) and the higher backscatter intensity signature observed in the pit (Fig. 8b).

A sediment sample retrieved from the sand waves adjacent to the scour pit contained fine sand (d_{50} = 0.104 mm) (Fig. 8a). As depositional signatures extending from wrecks usually consist of fine, redeposited sediments (Quinn, 2006; Raineault et al., 2013), here we assume that the depositional zone developed around the wreck consists of the same fine sand as the sand waves outside of the signatures (Fig. 8a).

The sand waves typically measure 10–15 m in length and 0.2–0.5 m in height and are pervasive around the wreck, but not developed within

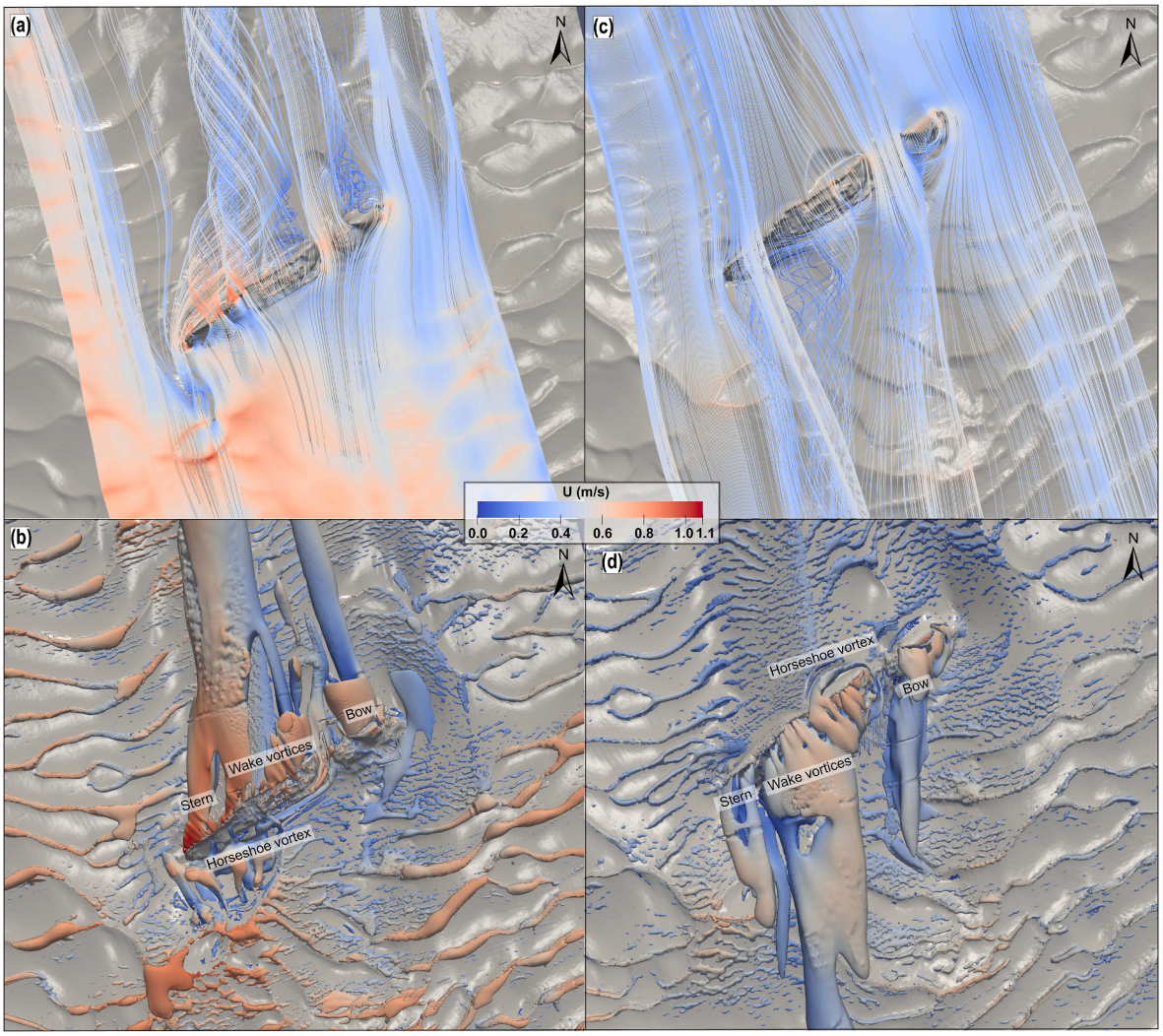

Fig. 7. Simulated flow patterns for the SS W.M. Barkley site. (a) Flow streamlines and (b) Q iso-surface (Q=0.0001) under the NNW current, (c) flow streamlines and (d) Q iso-surface under the SSE current.

the main scour pit. Their dominant propagation direction is aligned with the stronger SSE current modelled for the site (reaching a maximum speed of 0.90 m/s). However, this is reversed NNW of the main axis of the wreck, at the rim of the scour pit, similar to the pattern observed at the SS *W.M. Barkley* site (Fig. 8a). A large relict sand wave envelops the northern part of the scour pit, with a crest 13 m higher than the scour pit surface.

4.2.2. Geomorphic change

The high-resolution bathymetric surveys conducted at the HMS *Vanguard* site enabled evaluation of long-term bathymetric differences between 2015 and 2019 (Fig. 9). The vast, comet-shaped scour pit remained largely unaltered over the four years, with no detectable change over 81.1% of the area (Fig. 9a and b) and no change in the maximum scour depth. Some submetre changes are evidenced by the difference model in the area immediately surrounding the wreck, extending from its mast (−0.5 m) and near the portside (±0.7 m). Nevertheless, the majority of detectable geomorphic change was recorded outside of the pit and is associated with the migrating sand waves. In terms of areal coverage, erosion and deposition covered 5.7% and 13.2% of the area, respectively.

4.2.3. Structural change

The mean volumetric density within 1 m radius spheres of the point clouds obtained for HMS *Vanguard* in 2015 and 2019 was 483 and 515, respectively. The very high density of the points allowed for the visualization of the wreck's structure, containing a high level of detail, not only preserving major structural features, but also details like a hole created as a result of the impact of HMS *Iron Duke* and many deck elements including an anchor, funnel hole and gunwales (Fig. 10a).

Five regions of structural change are captured in the M3C2 difference model. The first region comprises a bending portside gunwale, which was displaced downwards by approximately 1.5 m (Fig. 10c, box 1). The second region is associated with one of the stern gunwales sliding down 1 m towards the seabed (Fig. 10c, box 2). The third and fourth regions are related to the iron mainmast lowering slightly (by approximately 0.3 m). This change in the mainmast's position is associated with erosion of the seabed around its tip (Fig. 10c, boxes 3,4 and Fig. 9a). Finally, highly localized, but potentially high magnitude (−2.5m) changes are registered on the upper surface of the box battery (Fig. 10c, box 5), which could be caused by plating falling into the hull, or like at the SS *W.M. Barkley*'s bow, uncertainties given the structural complexity.

4.2.4. Sediment mobility and wall shear stress

Grab sample and backscatter data indicate sandy sediment (mean d_{50} = 0.104 mm) dominates outside of the scour pit at the HMS *Vanguard* site, and gravel dominates within it. Different k_s values were therefore prescribed for the regions outside (corresponding to d_{50} =

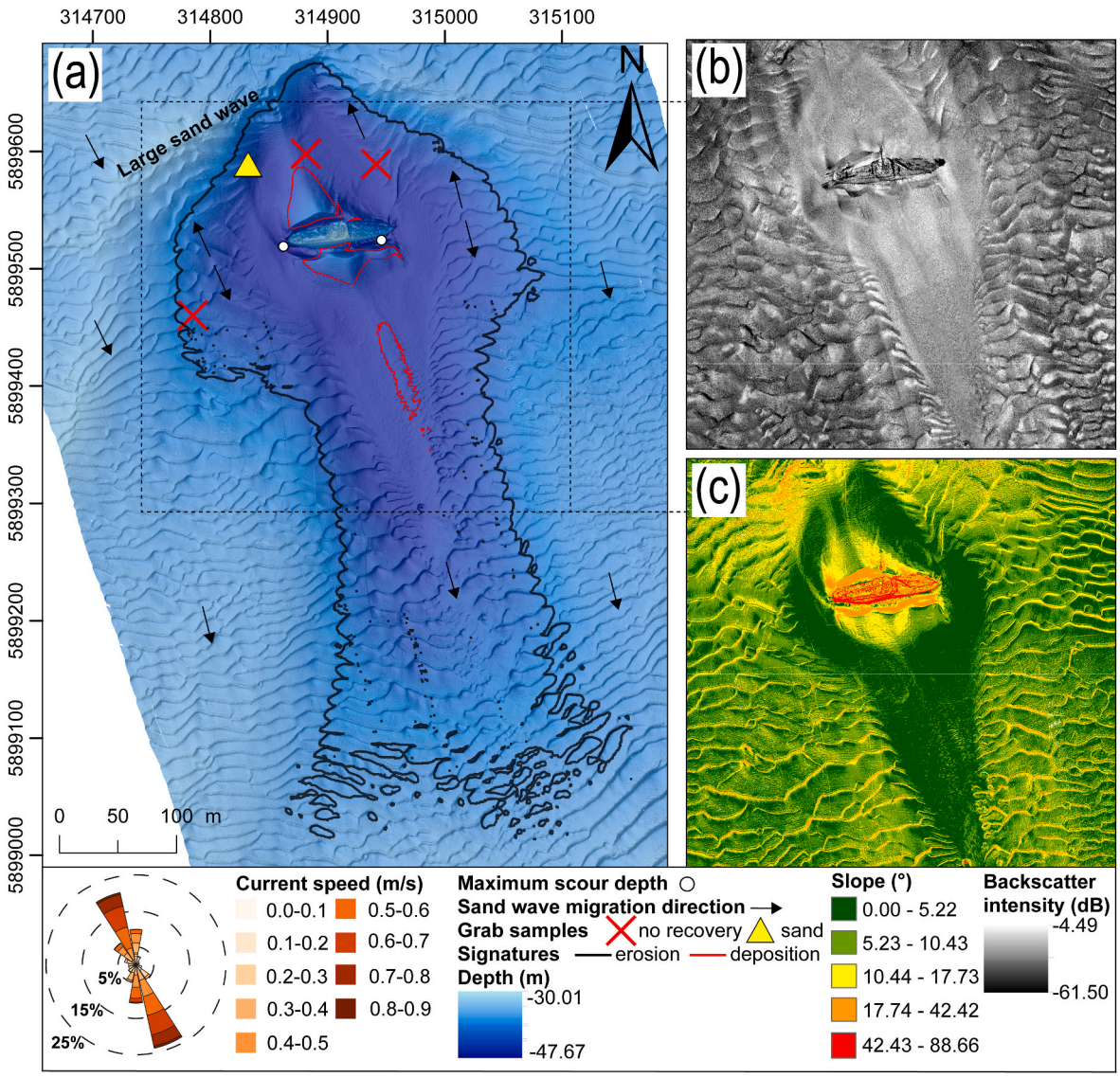

Fig. 8. Site characterization of the HMS Vanguard site. (a) Bathymetric DEM with the current rose obtained from the regional oceanographic model, (b) backscatter intensity mosaic, (c) slope map segregated using Jenks natural breaks optimization.

0.104 mm) and inside of the pit (d_{50} = 4 mm) and for the exposed wreck itself (smooth). The 90th percentiles of depth-averaged current speeds are 0.74 m/s and 0.73 m/s for the NNW and SSE directions, and equivalent velocity profiles were imposed at the inlets to the computational domains.

τ_c maps and frequency distributions for the HMS *Vanguard* site are presented in Fig. 11. As for the SS *W.M. Barkley* site, three wall shear stress groups were distinguished: low (below the τ_{cr} of fine sand; 0.14 Pa), moderate (between 0.14 Pa and 0.42 Pa) and high (all other values).

τ_{cr} for gravel (3.08 Pa) is not exceeded anywhere across the sites, including the area of the gravel bed (highlighted with the grey hatched area in Fig. 11 a andc) under NNW and SSE currents. This means that 42.0% and 64.2% of the total area is under no-exceedance conditions for the NNW and SSE current regimes, respectively. The remaining 58.0% and 35.8% of the areas, where the τ_{cr} exceedance was modelled, constitute the sand wave field outside of the scour pit (Fig. 11a) and some parts of the depositional zone (comprising fine sand), where the bed shear stress is amplified downstream of the wreck.

Simulations show the NNW current results in the development of a strong gradient of wall shear stress near the bow and stern (Fig. 11a). The elevated τ_c zone sourced at the bow reaches the end of the gravel bed and terminates nearby the stoss slope of the large sand wave NE of the wreck (Fig. 11a), while the ship's stern causes shear stress amplification reaching the NNW outlet of the computational domain. A mirrored distribution of shear stresses is observed under the SSE current regime. However, as there is no natural barrier SE (i.e. no large sand wave) of the wreck, τ_c amplification zones sourced at both tips of the wreck reach the outlet of the domain (Fig. 11c). τ_c is also amplified at the crests of the sand waves outside of the scour zone under both current regimes.

Concerning the shear stresses exerted at the shipwreck structure, high τ_c values are observed at the gunwales on the higher side of the wreck (portside) (Figs. 11a, box 1 and Fig. 11c, box 1). The SSE current also exerts increased shear stresses midships, at the box battery section (Fig. 11c, box 1), while the NNW current has a strong influence on the collapsed gunwale intersecting the stern section diagonally (Fig. 11a, box 1).

4.2.5. *Flow patterns*

The simulated NNW and SSE currents are orientated at 75° and 78° to the wreck of HMS *Vanguard*. Fig. 12 shows fully developed, averaged flow patterns at the site represented with flows streamlines and Q iso-

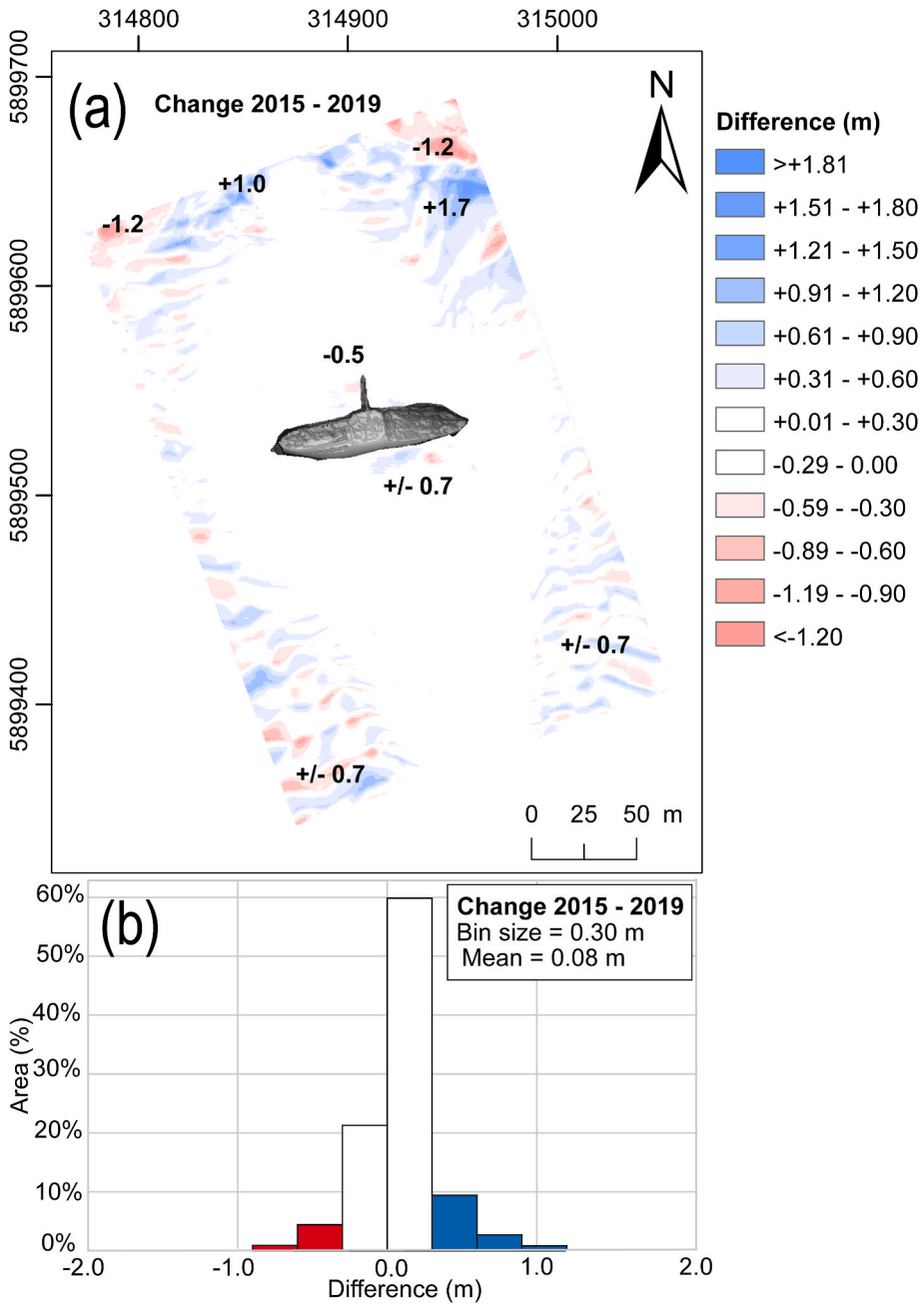

Fig. 9. Difference models for the HMS Vanguard site. (a) long-term model (2015-2019), (b) areal percentage histogram for the long-term model. Numbers on the difference model represent localised changes.

surface at Q = 0.0001 s^{-2}. The remarkable preservation of this nineteenth century shipwreck, retaining much of its original integrity on the seabed, causes substantial disruption to the tidal flows at the site.

Under the NNW current, a horseshoe vortex is clearly discernible in the Q iso-surface (Fig. 12b). It extends from the erosional trench, developed between the wreck and the depositional zone around it, and envelopes its structure, passing over the bow and stern with an overall asymmetric geometry, resulting from the wreck's oblique orientation towards the incoming flow. The vortex's diameter is larger at the inflow, stern side, and extends a shorter distance than at the bow. The wreck's structure poses a higher obstacle to the flow at the bow than at the partly collapsed stern section. The highest part of the wreck is at the armored box battery located midships. These irregularities in height, together with the shipwreck's list towards the starboard and the oblique incidence angle of flow, lead to an elaborate pattern of vortices developed over the wreck and in its wake (Fig. 12a and b). Separate vortices originate at the bow and stern sections of the wreck (Fig. 12a). Flow streamlines have a lower obstacle to overcome when passing through the collapsed stern and curl towards midships near the box battery (Fig. 12a). The stern- and bow- originating vortices merge downstream of the wreck to form a large asymmetric wake vortex. The complexity of the vortices is visible in the Q iso-surface, which captures their large, irregular and highly three-dimensional geometry (Fig. 12b).

The horseshoe vortex developed under the SSE current does not envelop the entire hull, unlike under the NNW current regime (Fig. 12 c and d). The collapsed stern section lists towards the oncoming SSE flow, presenting a surface with a shallower gradient (Fig. 12c and d) than the near vertical face presented to the flow in the opposite direction (Fig. 12a and b). This causes the inflow arm of the horseshoe vortex to pass over the wreck above the stern, rather than at the seabed around it.

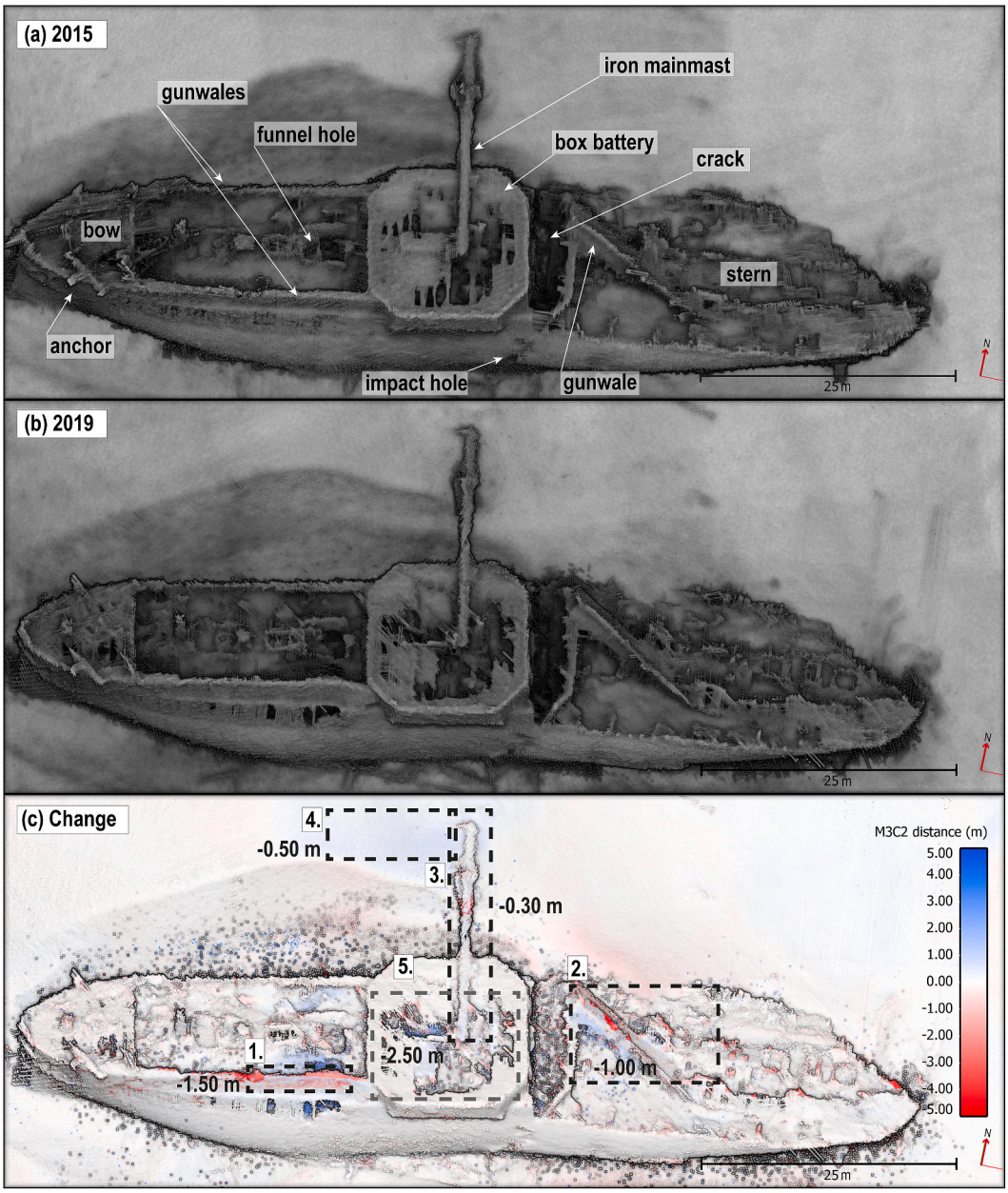

Fig. 10. Structural change model for the HMS Vanguard site. (a) point cloud corresponding to the 2015 survey, (b) point cloud corresponding to the 2019 survey , (c) difference model for the interval 2015-2019. Black and grey dashed lines represent certain and uncertain changes respectively.

On the other hand, at the bow side, the vortex passes under the bow's tip and extends further downstream, similar to that under the NNW flow regime. The SSE flow causes similar, complex and asymmetric distribution of wake vortices. Under the NNW current, the wake vortices form on the portside of the hull and cover the deck along the full length of the vessel (Fig. 12b). When the current approaches from the opposite direction, vortices are formed at the far side of the wreck, leaving the deck area unimpacted (Fig. 12d). Again, this is related to the fact that the wreck presents a less substantial, smoother obstacle for the SSE flow due to its starboard list, resulting in delayed flow separation.

5. Discussion

We now discuss in more detail the contribution of CFD to understanding the processes driving observed geomorphic and structural changes, additional methodological considerations and, finally, the wider implications of this work for ocean engineering and heritage/environmental management.

5.1. CFD simulations and geomorphic change

Previous research has investigated the role of wreck orientation relative to incoming steady flows using CFD (De Hauteclocque et al., 2007; Quinn and Smyth, 2018) and compared geomorphic changes with modelled flows at shipwreck sites using lower resolution bathymetric data (Fernández-Montblanc et al., 2018; Smyth and Quinn, 2014). However, the diverse geomorphology, structural complexity of the shipwreck sites, and the very high-resolution nature of the input DEMs investigated here result in the development of intricate flow and geomorphic change patterns, which have not been realised in previous studies. The novel combination of very high-resolution spatial and temporal datasets with CFD and sediment data allowed for a holistic investigation of these patterns.

Notably, wall shear stress is amplified by a factor of 4–5 due to the

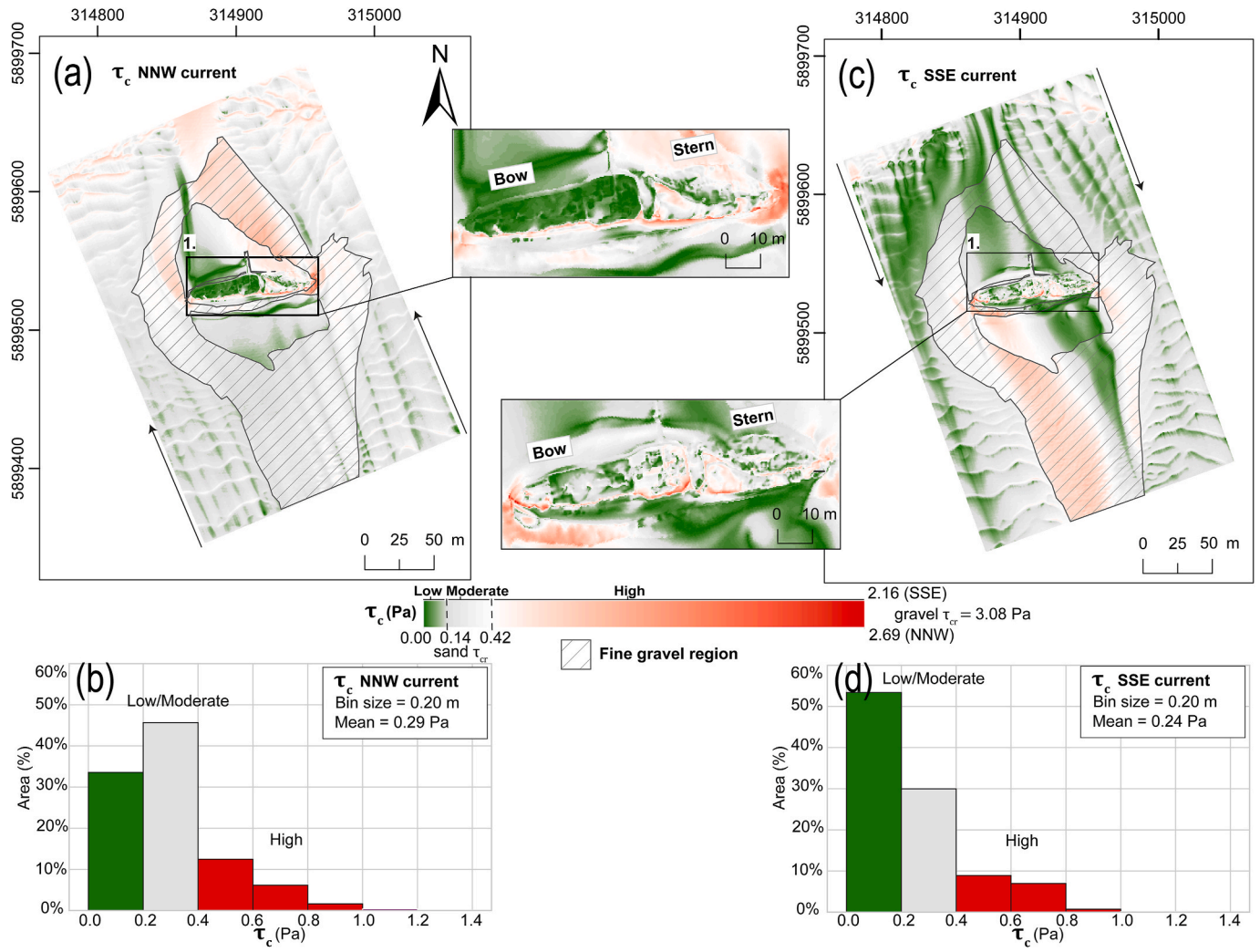

Fig. 11. Simulated wall shear stress maps for the HMS Vanguard site. (a) Wall shear stress under the NNW current with (1) close-up on the wreck, (b) areal percentage histogram for the wall shear stress values under the NNW current, (c) wall shear stress under the SSE current with (1) close-up on the wreck, (d) areal percentage histogram for the wall shear stress values under the SSE current.

interaction of flow with both shipwrecks, which is in close agreement with previous studies of flows at shipwreck sites (Smyth and Quinn, 2014) and other underwater structures (Sumer et al., 1997; Whitehouse, 1998). Vortex shedding and the formation of a pair of counter-rotating, low-velocity vortices simulated downstream of wrecks at incidence angles of 75° observed in previous models by Quinn and Smyth (2018) are absent at our sites despite their orientations (*Barkley*: 75°- 78°, *Vanguard:* 69°-68°). Flow and the associated vorticial patterns simulated for HMS *Vanguard* are more similar to those simulated by Quinn and Smyth (2018) for a 60° incidence angle. This discrepancy may be due to the fact that, while Quinn and Smyth (2018) used an upright hull structure in their simulations, the hull of HMS *Vanguard* lists to starboard, and is located in a topographic low (i.e. the scour depression), influencing flow separation. The flow separation is stronger for the upright hull of Quinn and Smyth (2018), and results in the development of the pair of counter-rotating vortices. Similarly, the list of SS W.M. Barkley, its irregular morphology (the wreck is broken into two), and emplacement within a deep scour pit causes the development of more complex flow and vortex patterns, but counter-rotating vortices are not observed, despite the wreck's orientation. Flow and wall shear stress patterns are discussed below for both sites in the context of geomorphic change recorded in the difference models.

5.1.1. SS W.M. Barkley

High-magnitude geomorphic change is recorded nearly everywhere in both the 4-year and one-week difference models. This corresponds well to the modelled τ_{cr} exceedance at the site (90.1% and 68.0% of the total area under the NNW and SSE currents). Therefore, it is evident that SS *W.M. Barkley* is in a live-bed scour regime (Whitehouse, 1998) under the simulated spring tide currents. This process is also reflected in sand wave migration everywhere across the site, including within the scour pits.

The most substantial changes are in the area immediately surrounding the shipwreck, causing reorganisation of the scour pits and an increase of the maximum scour depth by 1.01 m. This may be explained by several factors, some possibly inter-related. Firstly, it could be that the maximum scour depth has not yet been reached, despite the wreck resting on the seabed for 102 years. Secondly, occasional high-intensity storm surges could cause increased erosion. Thirdly, the changing morphology of the disintegrating wreck structure may directly affect scour processes and patterns. Fourthly, the migrating sand dunes, which move sediment through the system, may cause dynamic reorganisation of the pits. Finally, unsteady behaviour and flow turbulence could lead to temporary fluctuations in seabed levels.

Most probably, the recorded changes and the observed distribution of the scour and depositional signatures results from some combination of these factors. However, the first possibility is unlikely, as the time of

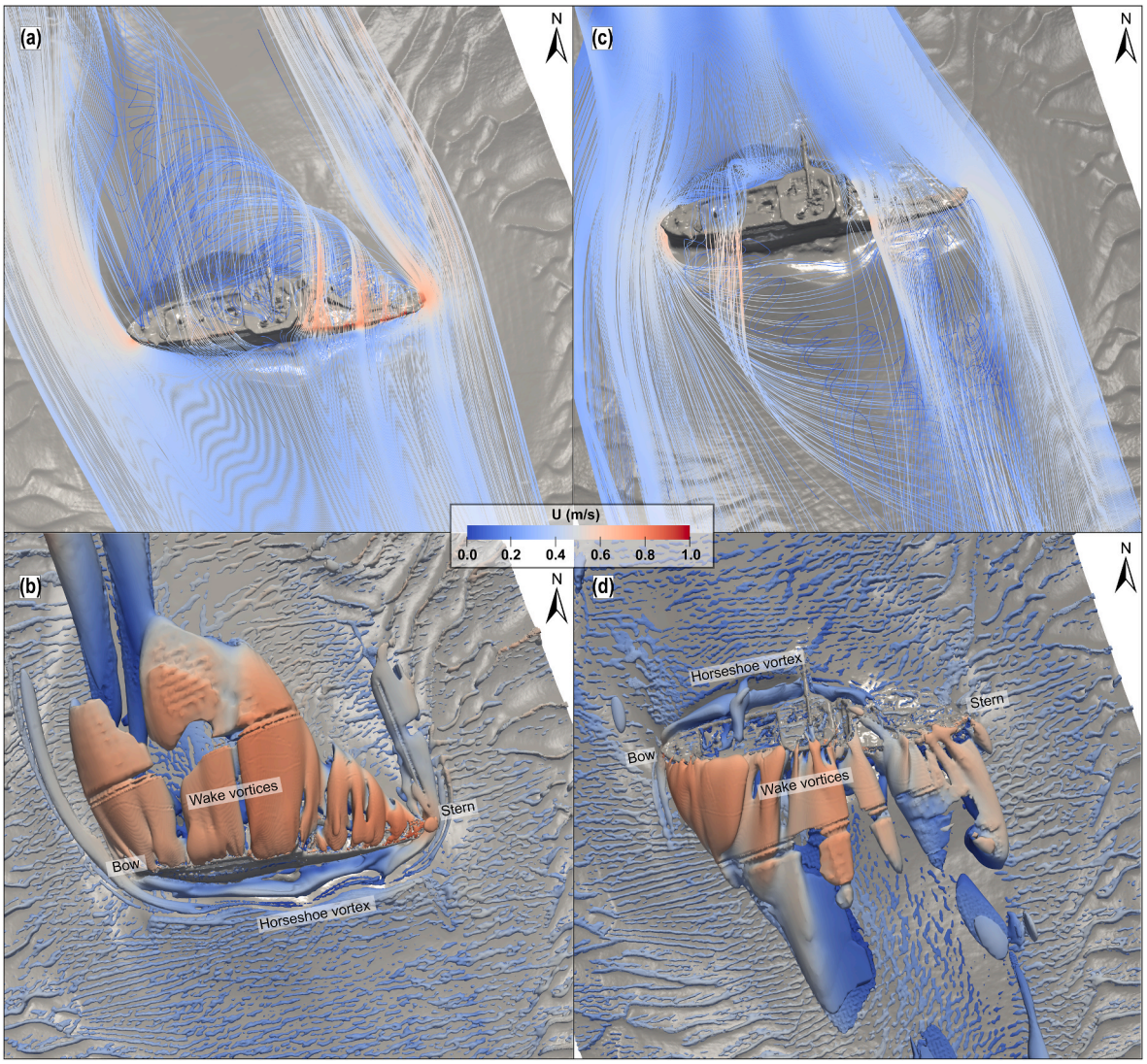

Fig. 12. Simulated flow patterns for the HMS Vanguard site. (a) Flow streamlines and (b) Q iso-surface (Q=0.0001) under the NNW current, (c) flow streamlines and (d) Q iso-surface under the SSE current.

the scour development would greatly exceed previously reported time-scales of scour reaching equilibrium depths at underwater structures (Raineault et al., 2013; Whitehouse, 1998; Whitehouse et al., 2011; Yao et al., 2021). According to Whitehouse (1998) the equilibrium scour depth, S_e, at a single vertical pile with a diameter D can be described using the relation $S_e/D = 1.3$, under the live-bed scour condition. SS *W.M. Barkley* is approximately 10 m wide and the average maximum scour depth (for the years 2015 and 2019) is 13.47 m. Despite the complexity of the shipwreck's structure compared to a monopile, these values compliment the relation of Whitehouse (1998), suggesting that the 1.01 m increase in scour pit depth may be a temporary fluctuation, rather than ongoing deepening. The simulated τ_c values are also low to moderate in the part of the pit where the maximum scour depth is recorded (Fig. 6a and c; Fig. 3a). Majcher et al. (2021) analysed longer time-lapse intervals and observed that between 2010 and 2015, the scour pit extending from the wreck's bow (Fig. 3) was infilled by sediments, rather than eroded further as shown in Fig. 4a. However, in terms of volumetric (Majcher et al., 2021) and areal changes (Fig. 4b), the site seems to have a negative sediment budget, hence, whilst unlikely, the possibility that scour has not reached its maximum depth cannot be completely discarded.

The influence of combined tidal and storm surge currents on bed shear stresses exacerbating erosion or deposition of sediments (the second possibility) at the sites should be also considered. The short-term difference model created for the SS *W.M. Barkley* site (Fig. 4c) represents changes, which happened in the one-week period, when a storm happened (29.10–03.11.2019). While sand wave migration is visible all over the site, the scour pits remain either unchanged or the changes are within the measurement errors (centimetric). Majcher et al. (2021) determined that wave influence has been limited at both investigated sites based on calculations involving mean wave lengths and significant wave heights recorded by a buoy located in the study area. The analysis included the storm event, which happened between the surveys in 2019. The same study (Majcher et al., 2021) and the investigation of Coughlan et al. (2021) determined that tidal currents enable the live-bed condition more than 50% of time of the year at the seabed around the SS *W.M. Barkley* site, based on the ROMS model data (Nagy et al., 2020) used to establish initial conditions for the simulations presented in this study. The simulations presented herein confirm that live-bed conditions exist during spring tides. Nevertheless, although the site's geomorphic change seems to be controlled by tidal currents most of the time, non-linear tide-surge interactions are known to affect the Irish Sea (Jones and Davies, 2003; Olbert and Hartnett, 2010) and should be considered as a factor occasionally intensifying scour processes.

The third possibility, involving feedback loops between the changing morphology of the disintegrating wreck structure and geomorphic

changes is highly probable, considering the structural changes experienced by the wreck during the investigation timeframe (Fig. 5). Every change in the obstacle's morphology results in some modification of flow patterns and the associated horseshoe and wake vortices. The seabed around the obstacle, in turn, responds to flow modification and more material is either deposited or eroded.

Even though the influence of migrating bedforms on the morphology of scour signatures has been deemed insignificant in a case study at a wind farm site (Couldrey et al., 2020), the fourth possibility seems probable, as sand dune migration across the site and inside the scour pits is recorded even in the one-week time-lapse (Fig. 4c). Migration is strongly exacerbated downstream of the wreck under the NNW current regime (Fig. 4c), in the same area where the τ_c values are highly elevated (Fig. 6a). As shown in Fig. 3, south of the wreck, the sand waves migrate in the opposite direction to the other sand waves in the area. This occurs due to the presence of the wreck and the local τ_c amplification south of the wreck under the SSE current regime, which has a weaker overall influence at the site (hence the global sand wave migration is oriented towards NNW). Nevertheless, the elaborate pathways of the sand wave migration within the pits may have caused their shifts.

Alternatively, shifts in the seabed might have been caused by unsteady flow behaviour, specifically fluctuating velocity due to turbulence and vortices developed around the shipwreck. Under the NNW regime, the horseshoe vortex is developed inside a trench between the depositional signature and the wreck (Fig. 3a) and essentially prevents the wreck from being covered with sediments on its starboard side (Fig. 7b). Under the SSE regime, the horseshoe vortex is developed only midships, and this corresponds to the high wall shear stress exerted on the depositional zone near its portside (Fig. 6c, box 1) and subsequent erosion of sediments (Fig. 4a). High τ_c is also exerted downstream of the wreck on the depositional mound adjacent to the wreck's starboard, where the wake vortices are formed (Fig. 6c). In the same place, the highest bathymetric change (−4.9 m) is recorded between the years 2015 and 2019 (Fig. 4a). Altogether, the formation of vortices clearly influences the τ_c values around the wreck, which causes further reorganisation of sediments.

5.1.2. HMS Vanguard

In contrast to the *Barkley* site, at the HMS *Vanguard* site, the seabed is only highly mobile outside the main scour pit (Fig. 9a). According to the CFD simulations, τ_{cr} is not exceeded at the gravel bed, encompassing a significant portion of the computational domain. We propose that the site was initially characterised by live-bed scour conditions, which waned as the gravel lag was exposed by erosion. This resulted in the site reaching a somewhat combined clear-water and live-bed scour condition under strong spring tide currents, where no bedform migration is observed within the erosional signature but is observed elsewhere around the site.

However, τ_{cr} is exceeded at some parts of the depositional zone extending from both sides of the wreck (Figs. 8a and 11), where no geomorphic change is recorded (Fig. 9a). Although we assumed that the depositional zone consists of redeposited fine sand, it is possible that the sandy sediment is mixed with fine gravel from the main scour pit or contains a shell fraction (or a combination of both). McCarron et al. (2019) estimated that τ_{cr} of sand in sand-gravel mixtures can be increased by up to 75% due to the hiding-exposure effect, which modifies the critical shear stress of individual grain classes in sediment mixtures depending on the grain size distribution. Additionally, Whitehouse (1998) noted the influence of slope on the critical shear stress required to mobilise sediments, which can be described using the relation: $\tau_{\beta cr}/\tau_{cr} = sin(\Phi_i + \beta)/sin(\Phi_i)$, where $\tau_{\beta cr}$ is the corrected critical shear stress, β is the is the local bedslope in the along flow direction (in degrees) and Φ_i is the angle of repose (32° by default; Soulsby, 1997). The average slope within the depositional zones here (Fig. 8a and c) is 12.6°. Therefore, the relation suggests that the corrected critical shear stress required to mobilise sediments at the depositional zone, can be up to 32.5% higher. These factors combined may explain why the depositional zone remains largely unchanged over the survey period, despite the modelled critical shear stress exceedance.

Nevertheless, some localised geomorphic changes are visible around the wreck extending from its collapsed mainmast (−0.5 m) and at the portside (±0.7 m) (Fig. 9a). Both are most probably related to the development of vortices around the wreck, and in particular, horseshoe vortices (Fig. 12b and d). They envelop the wreck causing its entrenchment between the depositional zones, which would otherwise (with less developed horseshoe vortices) most probably partially bury its structure. The erosional change extending from the tip of the collapsed mainmast may have happened due to the lowering of the mainmast itself (Fig. 10c). Another possibility is that erosion of the sediment caused the displacement of the mast. Certainly, a feedback loop exists between these two processes and flow patterns, discussed in more detail below.

5.2. CFD simulations and structural change

To the authors' knowledge this is the first published investigation that attempts to correlate outputs from CFD simulations with recorded structural changes (deterioration) of historic shipwrecks. Here we discuss how the modelled flow patterns and distribution of wall shear stresses may have affected the wrecks. Simulated pressure distributions on the shipwreck structures are included to support this discussion. Of note, the complexity of the physical processes affecting the sites, which may involve storm surges, varying tidal currents, and destructive anthropogenic impacts (e.g., bottom trawling) cannot be neglected when discussing damage sustained by the wreck structures. The simulated spring tide currents cannot be considered as representative of this wide range of processes. Therefore, the CFD outputs are discussed here to identify simulated flow characteristics which may have contributed to the collapse of parts of the shipwrecks, rather than having directly caused the damage.

5.2.1. SS W.M. Barkley

The most substantial damage experienced by SS *W.M. Barkley* between 2015 and 2019 happened at the portside of the counter stern, where a significant portion of the gunwale collapsed and now leans against the seabed (Fig. 5b and c, box 1). This coincides with the area of the highest modelled mean wall shear stresses (Fig. 6a, box 1) under the NNW current regime. Additionally, strong flow separation and formation of wake vortices occurs over the gunwale (Fig. 7a and b) and the whole counter stern is exposed to the highest pressures of all the structural elements of the wreck (Fig. 13a, box 1). Clearly, flows had exerted increased friction (induced by wall shear stresses) and pressure drags on the gunwale during energetic tidal periods (i.e. spring tides). This may have gradually weakened it with the aid of corrosion, resulting in its failure, possibly during a storm event. Longer-term, the wreck's counter stern may be prone to further damage, ultimately leading to its complete collapse.

Although the damage sustained by the wreck's bow section (Fig. 5c, box 2) is deemed uncertain due to the subjectivity introduced during point cloud cleaning, increased wall shear stresses are modelled here under the SSE current regime (Fig. 6c, box 1). This part of the wreck is also highly exposed and therefore, these structural changes remain probable.

5.2.2. HMS Vanguard

During the 2015–2019 interval, HMS *Vanguard* sustained damage to three, possibly four, parts of its structure (Fig. 10c). The displacement of the portside gunwale near the box battery (Fig. 10c, box 1) can be correlated with the increased wall shear stresses exerted on elevated sections under both current regimes (Fig. 11a, box 1 and Fig. 11c, box 1). The change in the collapsed gunwale at the stern section (Fig. 10c, box 2) coincides with increased shear stresses under both current directions (Fig. 11a, box 1 and Fig. 11c, box 1) and with an elevated pressure zone

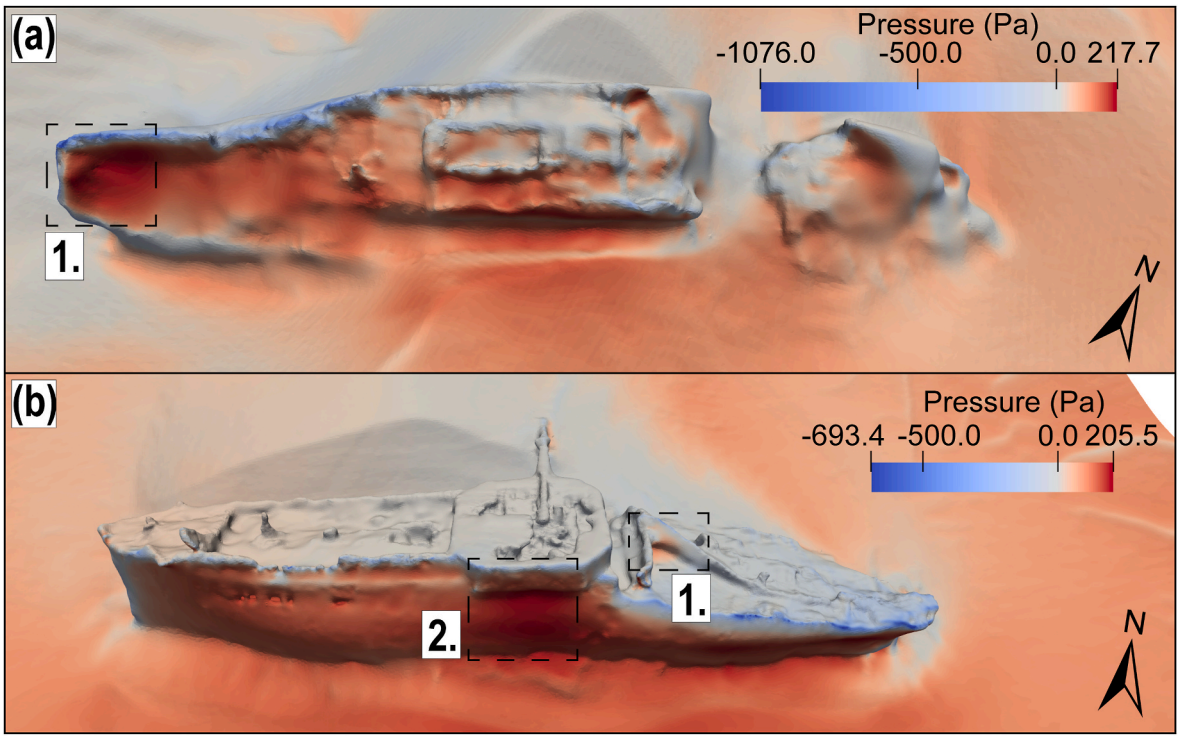

Fig. 13. Simulated pressure distributions under the NNW current regimes for the (a) SS W.M. Barkley site and (b) HMS Vanguard site. Hydrostatic pressure contribution is omitted.

(Fig. 13b, box 1). Similar to SS *W.M. Barkley*, the combination of these may have created a drag force causing gradual wear of the gunwale, contributing to its eventual displacement.

The wreck's mainmast, leaning on the seabed, has been lowered by approximately 0.30 m (Fig. 10c, box 3). Two mechanisms are possible here: either the mast was lowered before erosion of the seabed or seabed scour caused the lowering of the mast (Fig. 10c, boxes 3 and 4). As some seabed fluctuations are also recorded on the opposite side of the wreck (Fig. 9a), the scouring mechanism is probable. The complex arrangement of wake and horseshoe vortices (Fig. 12) (Dixen et al., 2013; Lee and Hong, 2019; Sumer et al., 1997), changing tidal currents (neap and spring) together with the possible influence of combined tidal and storm surge currents may have caused the changes in scour equilibrium, promoting further erosion at the mast's tip and its subsequent lowering.

Although the box battery changes could result from the point cloud cleaning (Fig. 10c, box 5), they are probably real considering the fragile state of its upper part. The upstanding, bluff body of the box battery is the highest part of the wreck and increased wall shear stresses are simulated at this structure under the SSE current (Fig. 11c, box 1). Even though this part of the shipwreck is very well preserved, the highest pressure is exerted on the portside of the hull under the box battery by the oncoming NNW current (Fig. 13b, box 2). The flow-exerted pressure together with the weight of the heavily armoured box battery and the existing hull damage (impact hole, crack across the stern; Fig. 10a) could contribute to an eventual collapse of the hull structure underneath, for example during a severe storm event.

5.3. Methodological considerations

Numerical modelling of fluid flows over any complex terrain involves multiple considerations (Blocken, 2018; Blocken et al., 2015; Grau-Bové et al., 2019; Smyth, 2016; Wakes et al., 2010). Our study has partially explored some of them, particularly in relation to obtaining current speed and direction in tidally-influenced moderate depth shelf-sea and mesh resolution for complex wreck structures. Additional remarks are made on structural change detection using high-resolution MBES data to supplement methodological considerations previously discussed in (Astley, 2016; Bates et al., 2011; Majcher et al., 2020; Plets et al., 2011; Quinn and Boland, 2010; Westley et al., 2019).

5.3.1. CFD simulations

The choice of initial conditions (i.e. input current velocity profiles, turbulence kinetic energy and dissipation rate and roughness length parameter) can inevitably influence the results of the simulations. Here we attempted to mimic real ocean conditions using all available information (i.e. regional ocean current data of Nagy et al. (2020), sediment data, high-resolution bathymetry). However, some simplifications and assumptions were necessary to make the modelling feasible. The choice of the 90th percentile current speed coming from two dominant directions obtained at one grid node of a regional scale oceanographic model is a simplification considering the tidal harmonics in the region (Lewis et al., 2015, 2017). Nevertheless, the results show good agreement between the observed geomorphological features (sand waves and scour marks), geomorphic changes and the modelled currents, suggesting that the chosen flow directions were suitable. The inlet velocity profiles and turbulence, which influence simulated wall shear stresses (used to assess sediment mobility) were also in agreement with presence and absence of geomorphic changes observed in the difference models. Another measure to improve the quality and accuracy of the simulations was to use the extended upstream fetch domains meshed over the regional bathymetry (Fig. 2) to develop the flows, before imposing the initial conditions at the inlets to the main computational domains.

Additionally, it is noted that the results of the grid independence study show some considerable (>1%) differences between flow variables modelled at the fine and medium resolution meshes (see supplementary material). Although these differences were deemed insignificant for the purpose of this research, guidelines and norms for achieving grid independence for this type of CFD simulation (i.e. involving highly complex topography derived from remote sensing data) should be established for standardization. Further refinement of CFD

domains here was deemed unfeasible, as the computational costs of multiple simulations performed in this study would become prohibitive.

Nevertheless, more research should be conducted into the influence of the choice of the turbulence closure, initial conditions and domain resolution on the results of site-scale underwater CFD simulations. Ideally, such investigations could not only be compared against observed geomorphic changes and geomorphology, but also validated with physical modelling (e.g. Yiannoukos et al., 2020) or with *in-situ* data (e.g. Unsworth et al., 2020), capturing speeds and directions of currents and flow turbulence at several strategic locations at a site.

5.3.2. Structural change

In this paper, dense, MBES-derived point clouds corresponding to repeat bathymetric surveys were used to assess changes in shipwreck structures. Although major structural changes were straightforward to validate in the difference models, some detected changes may be associated with the subjective point cloud cleaning process. Ideally, structural changes registered in such difference models should be further validated with either visual inspection by a diver or a remotely operated vehicle using video recording, photogrammetry or laser-line scanning techniques (Johnson et al., 2020). However such operations remain costly and difficult, especially at nearly intact metal-hulled wreck sites (e.g. Nornes et al., 2015) with low water visibility (e.g. Pacheco-Ruiz et al., 2018), and strong currents like the ones investigated here.

5.4. Implications

This investigation has clearly demonstrated the links which exist between the sediment- and hydro-dynamic environment and stability of complex underwater structures like shipwrecks. This was made possible through the multi-disciplinary methodology involving repeat, high-resolution hydrographic surveys designed to capture shipwreck sites at their full extent, CFD simulations with MBES data-derived stereolithography representations of the sites, regional ocean current data and sediment information obtained from grab samples.

Given that shipwrecks are of interest to multiple stakeholders in the marine environment, our methods and observation have applications in the following:

1. Distribution of simulated wall shear stresses and pressures at shipwreck structures gives hints about areas potentially prone to structural damage. Thus, CFD outputs in conjunction with bathymetry-derived models could inform more sophisticated engineering models involving finite element analysis (Foecke et al., 2010) to predict long-term deterioration.
2. The approach developed here could be used in heritage condition assessments to capture the physical state of historically significant sites, identify threats and assess the viability of long-term, *in-situ* preservation (Gregory, 2020; Gregory and Manders, 2015). Importantly, by incorporating high to very high-resolution data, it enables an empirical assessment of intra-site vulnerability (e.g. identification of damage to specific wreck elements), a level of detail which goes beyond many existing condition assessments. This in turn enables more precise assignation of responsive management actions, such as targeted recording of vulnerable structures.
3. Similarly, these observations can aid environmental risk assessments of potentially polluting wrecks, which should involve investigation of geohazards i.e. seabed stability, the influence of currents and waves (Goodsir et al., 2019; Hac and Sarna, 2021; Szafrańska et al., 2021; Ventikos et al., 2016) as well as ideally considering the stability of the wreck structure itself, and thus the likelihood of deterioration-induced pollution release.
4. Gathering information about the geotechnical parameters of the seabed is important for the developments of offshore infrastructure. Together with natural bedforms (Van Landeghem et al., 2009, 2012; Stow et al., 2009), shipwrecks act as proxies indicating dominant current directions (Caston, 1979; Garlan et al., 2015) and susceptibility of the seabed to scour when complex man-made objects are introduced. Detailed investigations as performed here can provide valuable information for planning new developments.
5. Taking into consideration all the points outlined above, the combined methodology can inform marine spatial planning, which should include shipwrecks as they are an inherent component of the underwater landscape (Papageorgiou, 2018).

6. Conclusion

In this study, we combined very high resolution repeat bathymetric surfaces and point clouds with modelled oceanographic current and sediment substrate data, to provide inputs for CFD simulations and assess how sediment- and hydro-dynamic settings affect wreck site stability. We demonstrated that this integrated methodology can be used to predict live-bed or clear-water scour conditions, which control geomorphic change at submerged wreck sites, and explain patterns of sediment erosion and deposition. Additionally, some interrelations between flow patterns, exerted wall shear stresses, pressures and structural changes (i.e. deterioration) in shipwrecks were observed, suggesting that the combination of methods can help to identify wreck parts prone for accelerated wear. We propose that the methods presented and resulting observations can not only aid archaeological assessments and management of potentially polluting shipwrecks, but also inform ocean engineering.

Funding

This investigation was supported by the Marine Institute of Ireland's ship-time programme's funded projects 'World War I shipwrecks in the Irish Sea: commemoration, visualization and heritage management' (CV15021, CV16031) and 'Geohazard investigation in the Irish Sea using seismic and seabed mapping techniques (GIST)' (CV19027) and an Ulster University Vice-Chancellor's Research Studentship to Jan Majcher.

CRediT authorship contribution statement

Jan Majcher: Conceptualization, Methodology, Software, Validation, Formal analysis, Investigation, Data curation, Writing – original draft, Visualization. **Rory Quinn:** Conceptualization, Methodology, Investigation, Resources, Writing – review & editing, Supervision, Project administration, Funding acquisition. **Thomas Smyth:** Methodology, Writing – review & editing, Supervision, Funding acquisition. **Ruth Plets:** Investigation, Writing – review & editing, Supervision, Funding acquisition. **Chris McGonigle:** Investigation, Writing – review & editing, Supervision, Funding acquisition. **Kieran Westley:** Investigation, Writing – review & editing, Funding acquisition. **Fabio Sacchetti:** Methodology, Software, Resources, Funding acquisition. **Mark Coughlan:** Resources, Writing – review & editing, Funding acquisition.

Declaration of competing interest

The authors declare that they have no known competing financial interests or personal relationships that could have appeared to influence the work reported in this paper.

Acknowledgments

We thank Alex Braun, Annika Clements, Shauna Creane, Mekayla Dale, Eoghan Daly, Megan Dolan, Cristiana Giglio, Rory McNeary, Rory O'Loughlin, Kevin Sheehan, and Viacheslav Sobolev for their assistance during and after the hydrographic surveys, to Cynthia Sassenroth and Mary Therese Kelly for conducting the sediment grain size analysis and to the crew of RV *Celtic Voyager* for their determination and passion

when performing the wreck surveys. Thanks are also extended to Bert Blocken for discussions about boundary conditions and to Colin Anderson who provided technical support with the high-performance computer. Additionally, we express gratitude to the MI Oceanographic Services Team for their timely support with our ocean current data requests. In the end, we thank two anonymous reviewers for insightful and very helpful reviews.

Appendix A. Supplementary data

Supplementary data to this article can be found online at https://doi.org/10.1016/j.oceaneng.2022.110625.

References

Astley, A.J., 2016. The Taphonomy of Historic Shipwreck Sites. University of Southampton.

Bates, C.R., Lawrence, M., Dean, M., Robertson, P., 2011. Geophysical methods for wreck-site monitoring: the rapid archaeological site surveying and evaluation (RASSE) programme. Int. J. Naut. Archaeol. 40, 404–416. https://doi.org/10.1111/j.1095-9270.2010.00298.x.

Blocken, B., 2018. LES over RANS in building simulation for outdoor and indoor applications: a foregone conclusion? Build. Simul. 11, 821–870. https://doi.org/10.1007/s12273-018-0459-3.

Blocken, B., 2015. Computational Fluid Dynamics for urban physics: importance, scales, possibilities, limitations and ten tips and tricks towards accurate and reliable simulations. Build. Environ. 91, 219–245. https://doi.org/10.1016/j.buildenv.2015.02.015.

Blocken, B., van der Hout, A., Dekker, J., Weiler, O., 2015. CFD simulation of wind flow over natural complex terrain: case study with validation by field measurements for Ria de Ferrol, Galicia, Spain. J. Wind Eng. Ind. Aerod. 147, 43–57. https://doi.org/10.1016/j.jweia.2015.09.007.

Blott, S.J., Pye, K., 2001. Gradistat: a grain size distribution and statistics package for the analysis of unconsolidated sediments. Earth Surf. Process. Landforms 26, 1237–1248. https://doi.org/10.1002/esp.261.

Brady, K., McKeon, C., Lyttleton, J., Lawler, I., 2012. Warships, U-Boats & Liners - A Guide to Shipwrecks Mapped in Irish Waters. The Stationery Office, Dublin.

Calder, B., Wells, D.E., 2007. CUBE User Manual. University of New Hampshire, Durham.

Carter, M., Goodsir, F., Cundall, P., Devlin, M., Fuller, S., Jeffery, B., Hil, G., Talouli, A., 2021. Ticking ecological time bombs: risk characterisation and management of oil polluting World War II shipwrecks in the Pacific Ocean. Mar. Pollut. Bull. 164, 112087. https://doi.org/10.1016/j.marpolbul.2021.112087.

Caston, G.F., 1979. Wreck marks: indicators of net sand transport. Mar. Geol. 33, 193–204. https://doi.org/10.1016/0025-3227(79)90080-X.

Coughlan, M., Guerrini, M., Creane, S., O'Shea, M., Ward, S.L., Van Landeghem, K.J.J., Murphy, J., Doherty, P., 2021. A new seabed mobility index for the Irish Sea: modelling seabed shear stress and classifying sediment mobilisation to help predict erosion, deposition, and sediment distribution. Continent. Shelf Res. 229, 104574. https://doi.org/10.1016/j.csr.2021.104574.

Coughlan, M., Long, M., Doherty, P., Coughlan, M., 2020. Geological and geotechnical constraints in the Irish Sea for offshore renewable energy energy. J. Maps 16, 420–431. https://doi.org/10.1080/17445647.2020.1758811.

Couldrey, A.J., Benson, T., Knaapen, M.A.F., Marten, K.V., Whitehouse, R.J.S., 2020. Morphological evolution of a barchan dune migrating past an offshore wind farm foundation. Earth Surf. Process. Landforms 45, 2884–2896. https://doi.org/10.1002/esp.4937.

Croome, A., 1999. Sinking fast. In: Rhind, D. (Ed.), Marine Industrial Technology. United Nations Industrial Development Organization (UNIDO), Vienna.

De Hauteclocque, G., Dix, J.K., Lambkin, D., Turnock, S., 2007. Flow and Likely Scour Around Three-Dimensional Seabed Structures Evaluated Using RANS CFD (Ship Science Report, vol. 144 (Southampton).

Dixen, M., Sumer, B.M., Fredsøe, J., 2013. Numerical and experimental investigation of flow and scour around a half-buried sphere. Coast. Eng. 73, 84–105. https://doi.org/10.1016/j.coastaleng.2012.10.006.

Elkin, D., Gutiérrez, G., Underwood, C.J., 2020. Metal shipwrecks in Patagonia, Argentina: contributions to their research and management. Int. J. Naut. Archaeol. 49, 303–317. https://doi.org/10.1111/1095-9270.12441.

EMODnet Bathymetry Consortium, 2018. EMODnet digital bathymetry (DTM 2018). https://doi.org/10.12770/18ff0d48-b203-4a65-94a9-5fd8b0ec35f6.

Evans, A.M., Firth, A., 2016. Anthropogenic impacts of development-led archaeology in an offshore context. In: Keith, M. (Ed.), Site Formation Processes of Submerged Shipwrecks. University Press of Florida, Gainesville, pp. 133–156.

Fernández-Montblanc, T., Izquierdo, A., Quinn, R., Bethencourt, M., 2018. Waves and wrecks: a computational fluid dynamic study in an underwater archaeological site. Ocean Eng. 163, 232–250. https://doi.org/10.1016/j.oceaneng.2018.05.062.

Fernández-Montblanc, T., Quinn, R., Izquierdo, A., Bethencourt, M., 2016. Evolution of a shallow water wave-dominated shipwreck site: fougueux (1805), gulf of cadiz. Geoarchaeology 31, 487–505. https://doi.org/10.1002/gea.21565.

Firth, A., 2018. Managing Shipwrecks. Fjord Limited for Honor Frost Foundation.

Foecke, T., Ma, L., Russell, M.A., Conlin, D.L., Murphy, L.E., 2010. Investigating archaeological site formation processes on the battleship USS Arizona using finite element analysis. J. Archaeol. Sci. 37, 1090–1101. https://doi.org/10.1016/j.jas.2009.12.009.

Folk, R.L., 1954. The distinction between grain size and mineral composition in sedimentary-rock. J. Geol. 62, 344–359.

Garlan, T., Marches, E., Brenon, E., 2015. A classification of scouring marks in macrotidal environments from analysis of long term wreck marks. In: Wang, P., Rosati, J.D., Cheng, J. (Eds.), The Proceedings of the Coastal Sediments 2015. World Scientific, Singapore, p. 14. https://doi.org/10.1142/9789814689977_0202.

Geraga, M., Christodoulou, D., Eleftherakis, D., Papatheodorou, G., Fakiris, E., Dimas, X., Georgiou, N., Kordella, S., Prevenios, M., Iatrou, M., Zoura, D., Kekebanou, S., Sotiropoulos, M., Ferentinos, G., 2020. Atlas of shipwrecks in inner ionian sea (Greece): a remote sensing approach. Heritage 3, 1210–1236. https://doi.org/10.3390/heritage3040067.

Ginsberg, S.S., Aliotta, S., 2019. Impact of a rocky outcrop on hydrodynamics and geomorphology in a mesotidal channel. Estuar. Coast Shelf Sci. 225, 106250. https://doi.org/10.1016/j.ecss.2019.106250.

Goodsir, F., Lonsdale, J.A., Mitchell, P.J., Suehring, R., Farcas, A., Whomersley, P., Brant, J.L., Clarke, C., Kirby, M.F., Skelhorn, M., Hill, P.G., 2019. A standardised approach to the environmental risk assessment of potentially polluting wrecks. Mar. Pollut. Bull. 142, 290–302. https://doi.org/10.1016/j.marpolbul.2019.03.038.

Grau-Bové, J., Mazzei, L., Strlic, M., Cassar, M., 2019. Fluid simulations in heritage science. Herit. Sci. 7, 1–12. https://doi.org/10.1186/s40494-019-0259-9.

Gregory, D., 2020. Characterizing the preservation potential of buried marine archaeological sites. Heritage 3, 838–857. https://doi.org/10.3390/heritage3030046.

Gregory, D., Manders, M., 2015. Guidelines to the Process of Underwater Archaeological Research, SASMAP Guideline Manual 1. SASMAP.

Grządziel, A., 2020a. Using remote sensing techniques to document and identify the largest underwater object of the Baltic sea: case study of the only German aircraft carrier, Graf Zeppelin. Rem. Sens. 12, 4076. https://doi.org/10.3390/rs12244076.

Grządziel, A., 2020b. Using remote sensing data to identify large bottom objects: the case of world war II shipwreck of general von Steuben. Geosciences 10, 1–15. https://doi.org/10.3390/geosciences10060240.

Guinan, J., McKeon, C., O'Keeffe, E., Monteys, X., Sacchetti, F., Coughlan, M., Nic Aonghusa, C., 2020. INFOMAR data in the EMODnet Geology data portal supports marine spatial planning and offshore energy development in the Irish offshore. Q. J. Eng. Geol. Hydrogeol. 54 https://doi.org/10.1144/qjegh2020-033.

Hac, B., Sarna, O., 2021. General Methodology of Oil Removal Operations on Baltic Shipwrecks. The MARE Foundation.

Hay, A.E., Speller, R., 2005. Naturally occurring scour pits in nearshore sands. J. Geophys. Res. Earth Surf. 110, 1–15. https://doi.org/10.1029/2004JF000199.

Howarth, M.J., 2001. Hydrography of the Irish sea, SEA6 technical report. POL Intern. Doc. 174.

Hunt, J.C.R., Wray, A.A., Moin, P., 1988. Eddies, streams, and convergence zones in turbulent flows. In: Studying Turbulence Using Numerical Simulation Databases, 2. Proceedings of the 1988 Summer Program. Center for Turbulence Research, pp. 193–208.

IHO, 2020. IHO Standards for Hydrographic Surveys. International Hydrographic Organization.

Issa, R.I., 1986. Solution of the implicitly discretised fluid flow equations by operator-splitting. J. Comput. Phys. 62, 40–65. https://doi.org/10.1016/0021-9991(86)90099-9.

Jackson, D.I., Jackson, A.A., Evans, D., Wingfield, R.T.R., Barnes, R.P., J, A.M., 1995. United Kingdom Offshore Regional Report: the Geology of the Irish Sea. British Geological Survey, London.

James, M.R., Robson, S., Smith, M.W., 2017. 3-D uncertainty-based topographic change detection with structure-from-motion photogrammetry : precision maps for ground control and directly georeferenced surveys. Earth Surf. Process. Landforms 42, 1769–1788. https://doi.org/10.1002/esp.4125.

Jenkins, S.A., Inman, D.L., Richardson, M.D., Wever, T.F., Wasyl, J., 2007. Scour and burial mechanics of objects in the nearshore. IEEE J. Ocean. Eng. 32, 78–90. https://doi.org/10.1109/JOE.2007.890946.

Johnson, K.H., Paxton, A.B., Taylor, J.C., Hoyt, J., McCord, J., Hoffman, W., 2020. Extracting ecological metrics from archeological surveys of shipwrecks using submersible video and laser-line scanning. Emerg. Technol. 11 https://doi.org/10.1002/ecs2.3210.

Jones, J.E., Davies, A.M., 2003. Processes influencing storm-induced currents in the Irish Sea. J. Phys. Oceanogr. 33, 88–104. https://doi.org/10.1175/1520-0485(2003)033<0088:PISICI>2.0.CO;2.

Kazhdan, M., Bolitho, M., Hoppe, H., 2006. Poisson surface reconstruction. Eurographics Symp. Geom. Process. 44, 61–70.

King, E.V., Conley, D.C., Masselink, G., Leonardi, N., McCarroll, R.J., Scott, T., 2019. The impact of waves and tides on residual sand transport on a sediment-poor, energetic, and macrotidal continental shelf. J. Geophys. Res. Ocean. 124, 4974–5002. https://doi.org/10.1029/2018JC014861.

Landquist, H., Hassellöv, I.M., Rosén, L., Lindgren, J.F., Dahllöf, I., 2013. Evaluating the needs of risk assessment methods of potentially polluting shipwrecks. J. Environ. Manag. 119, 85–92. https://doi.org/10.1016/j.jenvman.2012.12.036.

Lee, S.O., Hong, S.H., 2019. Turbulence characteristics before and after scour upstream of a scaled-down bridge pier model. Water (Switzerland) 11, 1–14. https://doi.org/10.3390/w11091900.

Lewis, M., Neill, S.P., Robins, P., Hashemi, M.R., Ward, S., 2017. Characteristics of the velocity profile at tidal-stream energy sites. Renew. Energy 114, 258–272. https://doi.org/10.1016/j.renene.2017.03.096.

Lewis, M., Neill, S.P., Robins, P.E., Hashemi, M.R., 2015. Resource assessment for future generations of tidal-stream energy arrays. Energy 83, 403–415. https://doi.org/10.1016/j.energy.2015.02.038.
Liu, B., Qu, J., Niu, Q., An, Z., Tan, L., 2021. Impact of anthropogenic activities on airflow field variation over a star dune. Catena 196. https://doi.org/10.1016/j.catena.2020.104877.
Lurton, X., Lamarche, G., 2015. Backscatter measurements by seafloor-mapping sonars: guidelines and recommendations, geohab report. https://doi.org/10.1007/978-3-642-01878-7_2.
Majcher, J., Plets, R., Quinn, R., 2020. Residual relief modelling: digital elevation enhancement for shipwreck site characterisation. Archaeol. Anthropol. Sci. 12 https://doi.org/10.1007/s12520-020-01082-6.
Majcher, J., Quinn, R., Plets, R., Coughlan, M., McGonigle, C., Sacchetti, F., Westley, K., 2021. Spatial and temporal variability in geomorphic change at tidally influenced shipwreck sites: the use of time-lapse multibeam data for the assessment of site formation processes. Geoarchaeology 36, 429–454. https://doi.org/10.1002/gea.21840.
Matutano, C., Negro, V., López-Gutiérrez, J.S., Esteban, M.D., 2013. Scour prediction and scour protections in offshore wind farms. Renew. Energy 57, 358–365. https://doi.org/10.1016/j.renene.2013.01.048.
MCA, 2018. UK Hydrography Programme. Survey Specification, Southampton.
McCarron, C.J., Van Landeghem, K.J.J., Baas, J.H., Amoudry, L.O., Malarkey, J., 2019. The hiding-exposure effect revisited: a method to calculate the mobility of bimodal sediment mixtures. Mar. Geol. 410, 22–31. https://doi.org/10.1016/j.margeo.2018.12.001.
McCartney, I., 2018. Scuttled in the Morning: the discoveries and surveys of HMS Warrior and HMS Sparrowhawk, the Battle of Jutland's last missing shipwrecks. Int. J. Naut. Archaeol. 47, 253–266. https://doi.org/10.1111/1095-9270.12302.
McCartney, I., 2017. The Battle of Jutland's heritage under threat: commercial salvage on the shipwrecks as observed 2000 to 2016. Mar. Mirror 103, 196–204. https://doi.org/10.1080/00253359.2017.1304701.
McNinch, J.E., Wells, J.T., Trembanis, A.C., 2006. Predicting the fate of artefacts in energetic, shallow marine environments: an approach to site management. Int. J. Naut. Archaeol. 35, 290–309. https://doi.org/10.1111/j.1095-9270.2006.00105.x.
Melling, G., 2015. Hydrodynamic and Geotechnical Control of Scour Around Offshore Monopiles. University of Southampton, Ocean and Earth Science.
Menter, F.R., Kuntz, M., Langtry, R., 2003. Ten years of industrial experience with the SST turbulence model. In: Hanjalic, K., Nagano, Y., Tummers, M. (Eds.), Turbulence, Heat and Mass Transfer 4. Begell House, Inc., pp. 625–632
Nagy, H., Lyons, K., Nolan, G., Cure, M., Dabrowski, T., 2020. A regional operational model for the north east atlantic: model configuration and validation. J. Mar. Sci. Eng. 8, 673. https://doi.org/10.3390/jmse8090673.
National Monuments Service, 1987. National Monuments (Amendment) Act, 1987. Republic of Ireland.
Neill, S.P., Hashemi, M.R., Lewis, M.J., 2014. Optimal phasing of the European tidal stream resource using the greedy algorithm with penalty function. Energy 73, 997–1006. https://doi.org/10.1016/j.energy.2014.07.002.
Nornes, S.M., Ludvigsen, M., Ødegård, Ø., Sørensen, A.J., 2015. Underwater photogrammetric mapping of an intact standing steel wreck with ROV. IFAC-PapersOnLine 48, 206–211. https://doi.org/10.1016/j.ifacol.2015.06.034.
O'Toole, R., Judge, M., Sachetti, F., Furey, T., Mac Craith, E., Sheehan, K., Kelly, S., Cullen, S., McGrath, F., Monteys, X., 2020. Mapping Ireland's coastal, shelf and deep water environments using illustrative case studies to highlight the impact of seabed mapping on the generation of blue knowledge. Geol. Soc. London, Spec. Publ. https://doi.org/10.1144/sp505-2019-207. SP505-2019–207.
Olbert, A.I., Hartnett, M., 2010. Storms and surges in Irish coastal waters. Ocean Model. 34, 50–62. https://doi.org/10.1016/j.ocemod.2010.04.004.
OpenCFD Ltd., 2019. OpenFOAM: user guide v2012 [WWW Document]. URL. https://www.openfoam.com/documentation/guides/latest/doc/index.html (accessed 6.23.21).
Ozer, J., Legrand, S., Od, R., Mumm, N., 2015. BEAWARE II: Review of the Physical Oceanography in the Area of the Bonn Agreement.
Pacheco-Ruiz, R., Adams, J., Pedrotti, F., 2018. 4D modelling of low visibility Underwater Archaeological excavations using multi-source photogrammetry in the Bulgarian Black Sea. J. Archaeol. Sci. 100, 120–129. https://doi.org/10.1016/j.jas.2018.10.005.
Papageorgiou, M., 2018. Underwater cultural heritage facing maritime spatial planning: legislative and technical issues. Ocean Coast Manag. 165, 195–202. https://doi.org/10.1016/j.ocecoaman.2018.08.032.
Plets, R., Quinn, R., Forsythe, W., Westley, K., Bell, T., Benetti, S., McGrath, F., Robinson, R., 2011. Using multibeam echo-sounder data to identify shipwreck sites: archaeological assessment of the joint Irish bathymetric survey data. Int. J. Naut. Archaeol. 40, 87–98. https://doi.org/10.1111/j.1095-9270.2010.00271.x.
Quinn, R., 2006. The role of scour in shipwreck site formation processes and the preservation of wreck-associated scour signatures in the sedimentary record - evidence from seabed and sub-surface data. J. Archaeol. Sci. 33, 1419–1432. https://doi.org/10.1016/j.jas.2006.01.011.
Quinn, R., Boland, D., 2010. The role of time-lapse bathymetric surveys in assessing morphological change at shipwreck sites. J. Archaeol. Sci. 37, 2938–2946. https://doi.org/10.1016/j.jas.2010.07.005.
Quinn, R., Smyth, T.A.G., 2018. Processes and patterns of flow, erosion, and deposition at shipwreck sites: a computational fluid dynamic simulation. Archaeol. Anthropol. Sci. 10, 1429–1442. https://doi.org/10.1007/s12520-017-0468-7.
Raineault, N.A., Trembanis, A.C., Miller, D.C., Capone, V., 2013. Interannual changes in seafloor surficial geology at an artificial reef site on the inner continental shelf. Continent. Shelf Res. 58, 67–78. https://doi.org/10.1016/j.csr.2013.03.008.
Roulund, A., Sumer, B.M., Fredsøe, J., Michelsen, J., 2005. Numerical and experimental investigation of flow and scour around a circular pile. J. Fluid Mech. 534, 351–401. https://doi.org/10.1017/S0022112005004507.
Shchepetkin, A.F., McWilliams, J.C., 2005. The regional oceanic modeling system (ROMS): a split-explicit, free-surface, topography-following-coordinate oceanic model. Ocean Model. 9, 347–404. https://doi.org/10.1016/j.ocemod.2004.08.002.
Shives, M., Crawford, C., 2014. Turbulence modelling for accurate wake prediction in tidal turbine arrays. In: 5th International Conference on Ocean Energy. Halifax.
Simpson, J.H., Crawford, W.R., Rippeth, T.P., Campbell, A.R., Cheok, J.V.S., 1996. The vertical structure of turbulent dissipation in shelf seas. J. Phys. Oceanogr. 26, 1579–1590. https://doi.org/10.1175/1520-0485(1996)026<1579:TVSOTD>2.0.CO;2.
Smyth, T.A.G., 2016. A review of Computational Fluid Dynamics (CFD) airflow modelling over aeolian landforms. Aeolian Res. 22, 153–164. https://doi.org/10.1016/j.aeolia.2016.07.003.
Smyth, T.A.G., Quinn, R., 2014. The role of computational fluid dynamics in understanding shipwreck site formation processes. J. Archaeol. Sci. 45, 220–225. https://doi.org/10.1016/j.jas.2014.02.025.
Soulsby, R., 1997. Dynamics of Marine Sands A Manual for Practical Applications. Thomas Telford.
Stow, D.A.V., Hernández-Molina, F.J., Llave, E., Sayago-Gil, M., Díaz-del Río, V., Branson, A., 2009. Bedform-velocity matrix: the estimation of bottom current velocity from bedform observations. Geology 37, 327–330. https://doi.org/10.1130/G25259A.1.
Sumer, B.M., 2007. Mathematical modelling of scour: a review. J. Hydraul. Res. 45, 723–735. https://doi.org/10.1080/00221686.2007.9521811.
Sumer, B.M., Christiansen, N., Fredsøe, J., 1997. The horseshoe vortex and vortex shedding around a vertical wall-mounted cylinder exposed to waves. J. Fluid Mech. 332, 41–70. https://doi.org/10.1017/s0022112096003898.
Sumer, B.M., Whitehouse, R.J.S., Tørum, A., 2001. Scour around coastal structures: a summary of recent research. Coast. Eng. 44, 153–190. https://doi.org/10.1016/S0378-3839(01)00024-2.
Sun, C., Lam, W.H., Dai, M., Hamill, G., 2019. Prediction of seabed scour induced by full-scale darrieus-type tidal current turbine. J. Mar. Sci. Eng. 7 https://doi.org/10.3390/jmse7100342.
Sweeney, M., Webb, R.M., Wilkinson, R.H., 1988. Scour around jackup rig footings. In: Offshore Technology Conference. https://doi.org/10.4043/5764-MS. Houston.
Szafrańska, M., Gil, M., Nowak, J., 2021. Toward monitoring and estimating the size of the HFO-contaminated seabed around a shipwreck using MBES backscatter data. Mar. Pollut. Bull. 171 https://doi.org/10.1016/j.marpolbul.2021.112747.
Testik, F.Y., Voropayev, S.I., Fernando, H.S., 2005. Flow around a short horizontal bottom cylinder under steady and oscillatory flows. Phys. Fluids 17. https://doi.org/10.1063/1.1868012.
UNESCO, 2017. Wrecks | united nations educational, scientific and cultural organization [WWW Document]. Wrecks. URL. http://www.unesco.org/new/en/culture/themes/underwater-cultural-heritage/underwater-cultural-heritage/wrecks/. accessed 4.13.21.
UNESCO, 2002. Records of the General Conference, 31st Session. October. UNESCO, Paris, pp. 50–61.
Unsworth, C.A., Nicholas, A.P., Ashworth, P.J., Best, J.L., Lane, S.N., Parsons, D.R., Sambrook Smith, G.H., Simpson, C.J., Strick, R.J.P., 2020. Influence of dunes on channel-scale flow and sediment transport in a sand bed Braided river. J. Geophys. Res. Earth Surf. 125 https://doi.org/10.1029/2020JF005571.
Van Der Vorst, H.A., 1992. Bi-CGSTAB: a fast and smoothly converging variant of Bi-CG for the solution of nonsymmetric linear systems. SIAM J. Sci. Stat. Comput. 13, 631–644.
Van Landeghem, K.J.J., Baas, J.H., Mitchell, N.C., Wilcockson, D., Wheeler, A.J., 2012. Reversed sediment wave migration in the Irish Sea , NW Europe : a reappraisal of the validity of geometry-based predictive modelling and assumptions. Mar. Geol. 295–298, 95–112. https://doi.org/10.1016/j.margeo.2011.12.004.
Van Landeghem, K.J.J., Wheeler, A.J., Mitchell, N.C., Sutton, G., 2009. Variations in sediment wave dimensions across the tidally dominated Irish Sea, NW Europe. Mar. Geol. 263, 108–119. https://doi.org/10.1016/j.margeo.2009.04.003.
Ventikos, N.P., Louzis, K., Koimtzoglou, A., Delikanidis, P., 2016. Enhanced decision making through probabilistic shipwreck risk assessment: focusing on the situation in Greece. Front. Mar. Sci. 3, 1–13. https://doi.org/10.3389/fmars.2016.00097.
Versteeg, H.K., Malalasekera, W., 2007. Conservation laws of fluid motion and boundary conditions, an introduction to computational fluid dynamics: the finite volume method. https://doi.org/10.2514/1.22547.
Wakes, S., 2013. Three-dimensional Computational Fluid Dynamic experiments over a complex dune topography. J. Coast Res. 165, 1337–1342. https://doi.org/10.2112/si65-226.1.
Wakes, S.J., Maegli, T., Dickinson, K.J., Hilton, M.J., 2010. Numerical modelling of wind flow over a complex topography. Environ. Model. Software 25, 237–247. https://doi.org/10.1016/j.envsoft.2009.08.003.
Ward, I.A.K., Larcombe, P., Veth, P., 1999. A new process-based model for wreck site formation. J. Archaeol. Sci. 26, 561–570. https://doi.org/10.1006/jasc.1998.0331.
Ward, S.L., Neill, S.P., Van Landeghem, K.J.J., Scourse, J.D., 2015. Classifying seabed sediment type using simulated tidal-induced bed shear stress. Mar. Geol. 367, 94–104. https://doi.org/10.1016/j.margeo.2015.05.010.
Weller, H.G., Tabor, G., Jasak, H., Fureby, C., 1998. A tensorial approach to computational continuum mechanics using object-oriented techniques. Comput. Phys. 12, 620. https://doi.org/10.1063/1.168744.
Westley, K., Plets, R., Quinn, R., McGonigle, C., Sacchetti, F., Dale, M., McNeary, R., Clements, A., 2019. Optimising protocols for high-definition imaging of historic

shipwrecks using multibeam echosounder. Archaeol. Anthropol. Sci. 11, 3629–3645. https://doi.org/10.1007/s12520-019-00831-6.

Wheaton, J.M., Brasington, J., Darby, S.E., Sear, D.A., 2010. Accounting for uncertainty in DEMs from repeat topographic surveys: improved sediment budgets. Earth Surf. Process. Landforms 35, 136–156. https://doi.org/10.1002/esp.1886.

Whitehouse, R.J.S., 1998. Scour at Marine Structures: a Manual for Practical Applications, Scour at Marine Structures: a Manual for Practical Applications. Thomas Telford, London. https://doi.org/10.1680/sams.26551.

Whitehouse, R.J.S., Harris, J.M., Sutherland, J., Rees, J., 2011. The nature of scour development and scour protection at offshore windfarm foundations. Mar. Pollut. Bull. 62, 73–88. https://doi.org/10.1016/j.marpolbul.2010.09.007.

Yao, W., Draper, S., An, H., Cheng, L., Harris, J.M., Whitehouse, R.J.S., 2021. Experimental study of local scour around submerged compound piles in steady current. Coast. Eng. 165, 103831. https://doi.org/10.1016/j.coastaleng.2020.103831.

Yiannoukos, I., Benson, T., Van Landeghem, K., Couldrey, A., Whitehouse, R., McCarron, C., Quinn, R., Morgan, J., Roberts, M., Clayton-Smith, B., 2020. Modelling scour around submerged objects with TELEMAC3D - GAIA. In: Breugem, W.A., Frederickx, L., Koutrouveli, T., Kulkarni, R., Chu, K., Decrop, B. (Eds.), Online Proceedings of the Papers Submitted to the 2020 TELEMAC-MASCARET User Conference. International Marine & Dredging Consultants, pp. 68–73.